Journal of Photochemistry & Photobiology, A: Chemistry 404 (2021) 112956

Contents lists available at ScienceDirect

Journal of Photochemistry & Photobiology, A: Chemistry

journal homepage: www.elsevier.com/locate/jphotochem

Quantum chemical computations, fluorescence spectral features and molecular docking of two biologically active heterocyclic class of compounds

Raveendra Melavanki [a,b,*,1], Kalpana Sharma [a], V.T. Muttannavar [c], Raviraj Kusanur [d,1], Kariyappa Katagi [e], Swarna M Patra [d], Siva Umapathy [f], Kishor Kumar Sadasivuni [g,**], Vikas M Shelar [h], Diksha Singh [h], NR Patil [i], Varsha V Koppal [i]

[a] Department of Physics, MS Ramaiah Institute of Technology, Bangalore, 560054, Karnataka, India
[b] Centre of Excellence for Imaging Technologies, MS Ramaiah Institute of Technology, Bangaluru, 560054, Karnataka, India
[c] Department of Physics, JSS Science RSH PU College, Vidyagiri, Dharwad, 580003, Karnataka, India
[d] Department of Chemistry, R.V. College of Engineering, Bangalore, Karnataka, India
[e] Department of Chemistry, Karnataka Science College, Dharwad, 580008, India
[f] Department of Inorganic and Physical Chemistry, Indian Institute of Science, Bangalore, Karnataka, India
[g] Centre for Advanced Materials, Qatar University, Doha, Qatar
[h] Department of Physics, MS Ramaiah University of Applied Science, Bengaluru, Karnataka, 560058, India
[i] Department of Physics, B.V.B. College of Engineering & Technology, Hubli, 580031, Karnataka, India

ARTICLE INFO

Keywords:
Solvatochromic method
Ground state and excited state dipole moments
DFT
NBO
MEP
Fukui functions
Molecular docking

ABSTRACT

This work is an effort for determination of excited and ground state values of dipole moments and also for quantum chemical computation of two biologically active heterocyclic class of compounds namely of 3-[2-Oxo-2-(2-oxo-2H-chromen-3-yl)-ethylidene]-1,3-dihydro-indol-2-one (3OCE) and 3-[2-Oxo-2-(3-oxo-3H-benzo[f]chromen-2-yl)-ethylidene]-1,3-dihydro-indol-2-one (3OBC). Redshift is displayed by both the compounds with some enhancement in polarity of solvent. The selected molecules show comparatively more polar nature in excited state than in ground state, and this is indicated by large dipole moment in the excited state. DFT calculations with B3LYP/6–311+G (d, p) basis sets using compound's quantum chemical property such as analysis of frontier molecular orbital were used for studying chemical reactivity and kinetic stability of selected compounds. MEP, NBO and Mulliken charges are further studied. The compounds exhibit great amount of energy for stabilization, which is depicted as transfer of proton showed by natural bond orbital (NBO) analysis within the selected donor-acceptor. The indices of electrophilicity and local softness of solute compounds being used is calculated with the help of Fukui function. In order to observe the biophysical properties of the compounds, molecular docking studies performed with periplasmic proteins (PDB ID: 2IPM and 2IPL).

1. Introduction

In biological and chemical sensors, molecular docking, there is a significant role of heterocyclic compounds like coumarin [1–3]. Medicinal chemists in past few decades, have been exploring synthetic and natural coumarin compounds for drug applications because of the interesting pharmacological properties of coumarin ring system. Coumarin compounds which were derived synthetically, namely pyrano coumarins, coumarin sulfamates and furano coumarins found applications as anti-inflammatory, antihypertensive, antibacterial, antitumor, anti-coagulant, photo chemotherapeutic, anti-HIV and antimicrobial agents. There are remarkable applications of these compounds in dye industries [3–5]. As there is a broad range of pharmaceutical and bio-chemistry applications, dipole moments comprehension has attracted large number of researchers in the recent years. The dipole moment estimation helps in studying distribution of charge, electron density,

* Corresponding author at: M.S. Ramaiah Institute of Technology, Bangalore, 560054, Karnataka, India.
** Corresponding author.
E-mail addresses: melavanki73@gmail.com (R. Melavanki), chishorecumar@gmail.com (K.K. Sadasivuni).
[1] (Affiliated to Visvesvaraya Technological University, Belagavi-590018, Karnataka, India).

https://doi.org/10.1016/j.jphotochem.2020.112956
Received 14 June 2020; Received in revised form 23 September 2020; Accepted 25 September 2020
Available online 30 September 2020
1010-6030/© 2020 Elsevier B.V. All rights reserved.

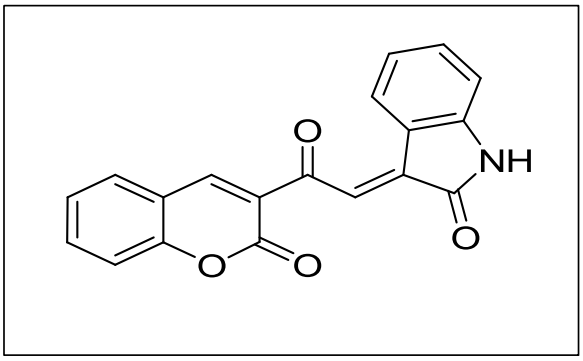

(a) 3OCE

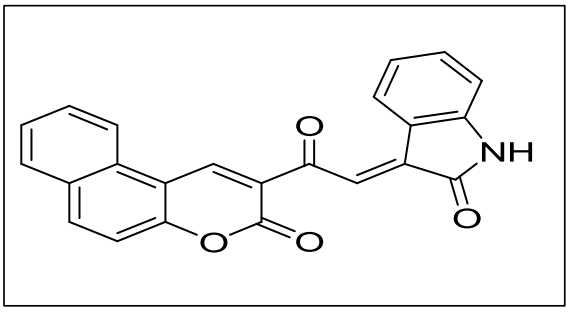

(b) 3OBC

Fig. 1. Molecular Structures of 1(a) 3OCE and 1(b) 3OBC.

geometrical structure in short lived state of fluorophore, etc.

Dipole moment for heterocyclic compounds are determined using a widely used solvatochromic method. There is a linear correlation between absorption and emission wave number and a polarity function for the solvent. Also, correlations are found between the theories of second order perturbation and that of quantum mechanical Onsager's reaction field [6–13]. In structural discovery, coumarin compounds are found to have an extensive significance [14–31]. For the design of new pharmaceutical compounds, the information on local reactivity descriptors based on charge density and molecular reactivity is provided by density functional theory (DFT) [32–66]. The motivation for our work on the fluorescence spectral features and quantum chemical computations of coumarin compounds came from literature survey of different heterocyclic compounds. In our study, we used the solvatochromic method for calculating the excited and ground state dipole moment of compounds 3OCE and 3OBC. Apart from that, quantum chemical computations were carried out using Gaussian 09 program like Mulliken charges, theoretical ground state dipole moment, NBO, MEP, NLO properties and Fukai calculations. Because of the polar nature and biological activity [65] of these coumarin compounds we planned to study the biophysical properties by docking with periplasmic proteins which are the major components of blood.

2. Materials and methods

2.1. Materials

By using standard methods, we synthesized two coumarin derivatives viz, 3-[2-Oxo-2-(2-oxo-2H-chromen-3-yl)-ethylidene]-1,3-dihydro-indol-2-one (3OCE) and 3-[2-Oxo-2-(3-oxo-3H-benzo[f]chromen-2-yl)-ethylidene]-1,3-dihydro-indol-2-one (3OBC) [63,65]. Solvents of different dielectric constant such as methanol (ML), acetonitrile (AN), ethanol (EL), dimethyl formamide (DMF), dimethyl sulphoxide (DMS), tetrahydrafuran (THF) and ethyl acetate (EA) are all of spectroscopic grade. All the mentioned solvents were obtained from S-D-Fine Chemicals Ltd., India. Fig. 1(a) & (b) shows molecular structure for compounds 3OCE and 3OBC. The molecular docking for both coumarin compounds were carried out using Auto Dock Tools version 1.5.6 software. The Best affinity mode of docked compound 3OCE and 3OBC with 2-IPM and IPL are as shown in Fig. 2(a) & (b) and Fig. 3(a) & 3(b)

2.2. Spectroscopic measurements

The fluorescence and absorption spectra of 3OCE and 3OBC are recorded in Hitachi F-2700 FL Spectroflourimeter and UV-3600 Spectrophotometer (Labomed) respectively at room temperatures. Preparation of fresh solution with concentration being 1×10^{-4} M is done in various solvents for both 3OCE and 3OBC compounds. The spectroscopic measurements are carried out with an instruments error of ±1 nm.

3. Results and discussion

3.1. Evaluating and investigating dipole moments for excited state and ground state through experimental approach

3.1.1. Determining the solvent effect on emission spectra and absorption spectra

The absorption spectra and emission spectra in 1,4 - dioxane solvent are shown in Fig. 4(a),(b) for 3OCE and Fig. 5(a),(b)for 3OBC compounds. Different spectral parameters for compounds 3OCE and 3OBC are illustrated respectively in Tables 1 and 2. It is observed that for both compounds the magnitude Stokes shift is positive. The observation indicates a dissimilar geometry and a less polar nature in ground state as compared in excited state. Hereby π→π* transition are confirmed for 3OCE and 3OBC compounds.

3.1.2. Determining dipole moment values for ground state and excited state by solvatochromic method

There are various methods to obtain the dipole moments for excited state and ground state. Those methods include solvatochromic effect, thermo chromic effect and electro chromic effect. Solvatochromic effect yields comparatively better results for wide range of compounds and so we used the same for our study. Solvatochromic shift method involves three independent equations [10–13] given as below

Lippert's equation [10],

$$\left(\bar{\nu}_a - \bar{\nu}_f\right) = m_1 F_1(\varepsilon, n) + constant \tag{1}$$

Bakhshiev's equation [11]

$$(\bar{\nu}_a - \bar{\nu}_f) = m_2 F_2(\varepsilon, n) + constant \tag{2}$$

Kawski-Chamma-Viallet'sequation [12,13]

$$\frac{(\bar{\nu}_a + \bar{\nu}_f)}{2} = m_3 F_3(\varepsilon, n) + constant \tag{3}$$

Where F_1, $F_2$and F_3 represents parameters for solvent polarity and can be expressed as

$$f_1(n,\varepsilon) = \left[\left(\frac{(\varepsilon-1)}{(2\varepsilon+1)}\right) - \left(\frac{(n^2-1)}{(2n^2+1)}\right)\right] \tag{4}$$

$$f_2(n,\varepsilon) = \left[\frac{(2n^2+1)}{(n^2+2)}\right]\left[\left(\frac{\varepsilon-1}{\varepsilon+2}\right) - \left(\frac{n^2-1}{n^2+2}\right)\right] \tag{5}$$

$$f_3(n,\varepsilon) = \left\{\frac{1}{2}\frac{(2n^2+1)}{(n^2+2)}\left[\frac{\varepsilon-1}{\varepsilon+2} - \frac{n^2-1}{n^2+2}\right] + \frac{3}{2}\left[\frac{n^4-1}{(n^2+2)^2}\right]\right\} \tag{6}$$

where

$\bar{\nu}_a$ –represents maxima wavenumber in absorption spectrum

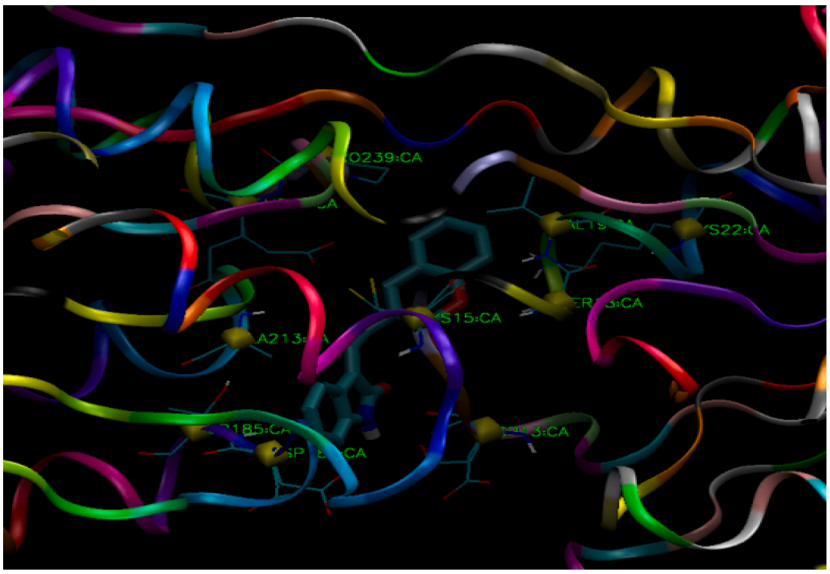

(a)

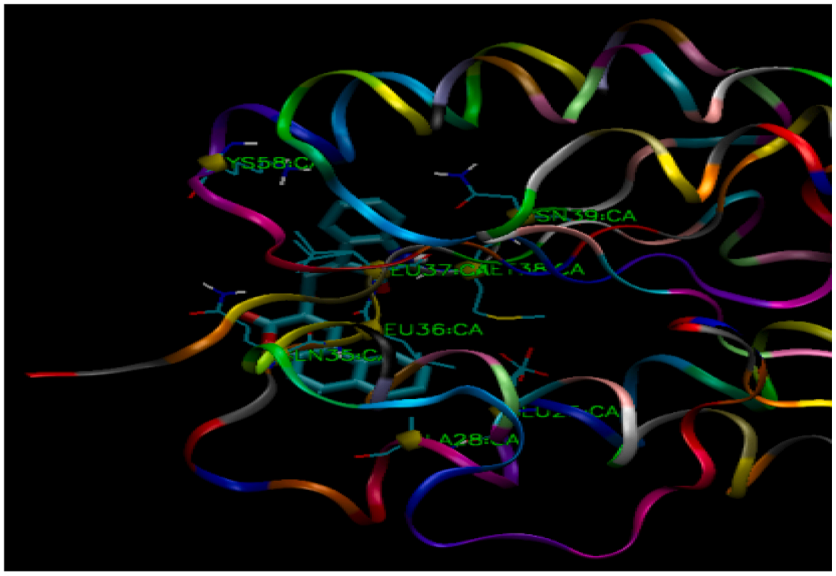

(b)

Fig. 2. Best affinity mode of docked compound 3OCE and 3OBC with 2-IPM.

$\bar{\nu}_f$ – (in cm^{-1}) represents maxima wavenumber in emission spectra.
n –solvent refractive index
ε - solvent dielectric constant

Tables 1–3 summarize different photophysical parameters of compounds 3OCE and 3OBC in different solvents. Figs. 6–8 (a),(b), (a),(b), (a),(b) show the linear graphs for $(\bar{\nu}_a - \bar{\nu}_f)$ v/sF_1 (ε, n), $(\bar{\nu}_a - \bar{\nu}_f)$ v/s F_2 (ε, n) and ½$(\bar{\nu}_a + \bar{\nu}_f)$ v/s F_3 (ε, n).Eqs. (1) – (3) are subjected to linear fitting to obtain slopes m_1, m_2 and m_3 respectively. These slopes are affected by the cavity radius size (a) and change in the value of dipole moment of the solute upon excitation ($\Delta\mu = \mu_e - \mu_g$). These can be represented as

$$m_1 = \frac{2(\mu_e - \mu_g)^2}{hca^3} \quad (7)$$

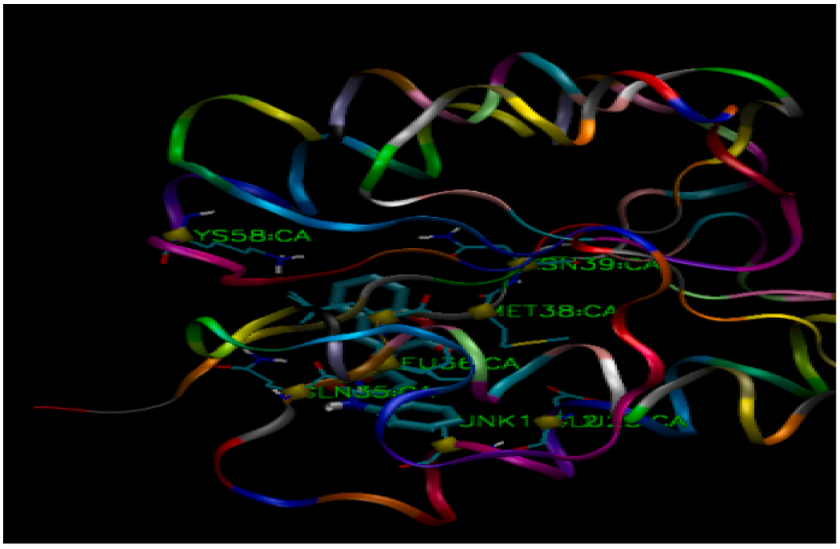

(a)

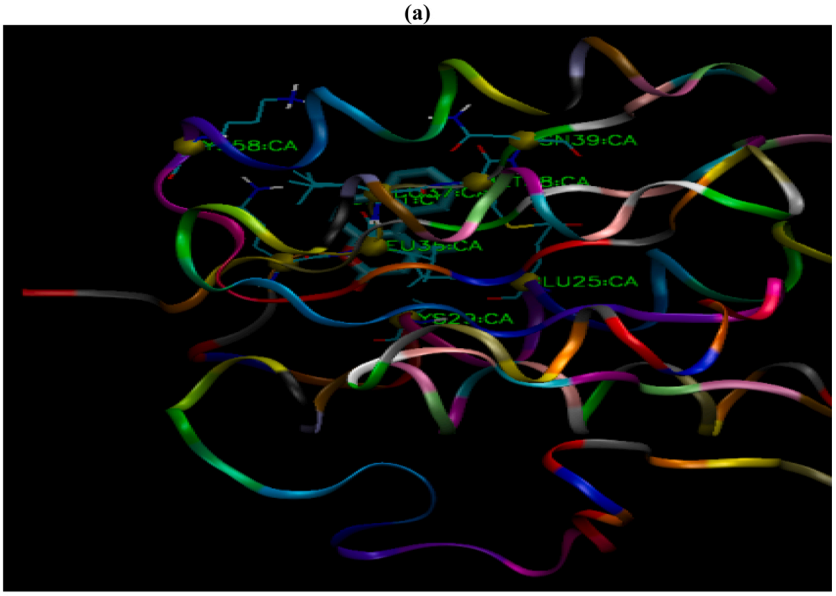

(b)

Fig. 3. Best affinity mode of docked compound 3OCE and 3OBC with 2-IPL.

$$m_2 = \frac{2(\mu_e - \mu_g)^2}{hca^3} \tag{8}$$

$$m_3 = \frac{2(\mu_e{}^2 - \mu_g{}^2)}{hca^3} \tag{9}$$

where,

μ_g refers to dipole moment at ground state, μ_e is the dipole moment at excited state, h represents planck's constant, c is the speed of light, "a'' represents the Onsager cavity radius [63] of the solutes. Table 4, depicts the solvents spectral shifts of 3OCE and 3OBC for various statistical correlations. Eqs. (10) – (12) is used for the determination of μ_g and μ_e provided that both are parallel to each other.

$$\mu_g = \frac{m_3 - m_2}{2}\left(\frac{hca^3}{2m_2}\right)^{\frac{1}{2}} \tag{10}$$

$$\mu_e = \frac{m_3 + m_2}{2}\left(\frac{hca^3}{2m_2}\right)^{\frac{1}{2}} \tag{11}$$

and

$$\mu_e = \frac{m_2 + m_3}{m_3 - m_2}\mu_g \; ; m_3 > m_2 \tag{12}$$

In general, angle between μ_g and μ_e are collinear [51–53], otherwise,

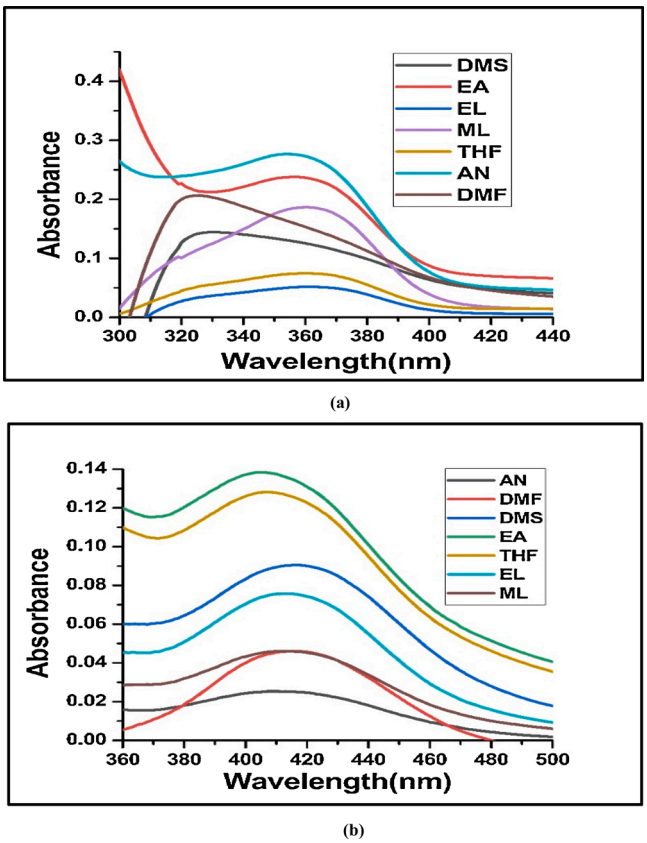

Fig. 4. Typical absorption spectrum of (a) 3OCE and (b) 3OBC in different solvents.

it is determined by equation given below

$$cos\varphi = \frac{1}{2\mu_g\mu_e}\left[\left(\mu_g{}^2+\mu_e{}^2\right)-\frac{m^{(3)}}{m^{(2)}}\left(\mu_e{}^2-\mu_g{}^2\right)\right] \quad (13)$$

Table 5 lists all different factors of dipole moment of compounds 3OCE and 3OBC. It is observed that, polar nature of solutes in ground state is lower than that in excited state which is indicated by μ_e being greater than μ_g but in case of 3OBC theoretical μ_g is high due to gas phase studies. Studies have shown that, after excitation there is an increase in dipole moment which helps to understand twisted intra-molecular charge transfer (TICT) character for excited species [20,29]. A good agreement was observed for μ_g and μ_e values estimated by the used methods. The difference between the values obtained from the spectral method and the theoretical calculation indicated that the occurrence of the TICT induced by the solvent effect is critical and the presence of some important factors such as hydrogen bonding interaction should be considered [66]. Whereas, angle between μ_g and μ_e is found to be 0° for both 3OCE and 3OBC. It hereby confirms the dipole moments to be collinear. All the obtained results agree with the literatures [9,16,24,28,29].

3.1.3. Molecular-microscopic solvent polarity parameter (E_T^N)

Microscopic solvent polarity parameter (E_T^N) is employed to understand the effect of polarization and H-bonding effect on the spectral properties which are neglected in the above theories. The relevant empirical formula as derived by Reichardt [54 and 55] for the correlation of the spectral shift with E_T^N, takes the form of

$$\overline{\nu}_a-\overline{\nu}_f = 11307.6\left[\left(\frac{\Delta\mu}{\Delta\mu_b}\right)^2\left(\frac{a_B}{a}\right)^3\right]E_T^N + constant \quad (14)$$

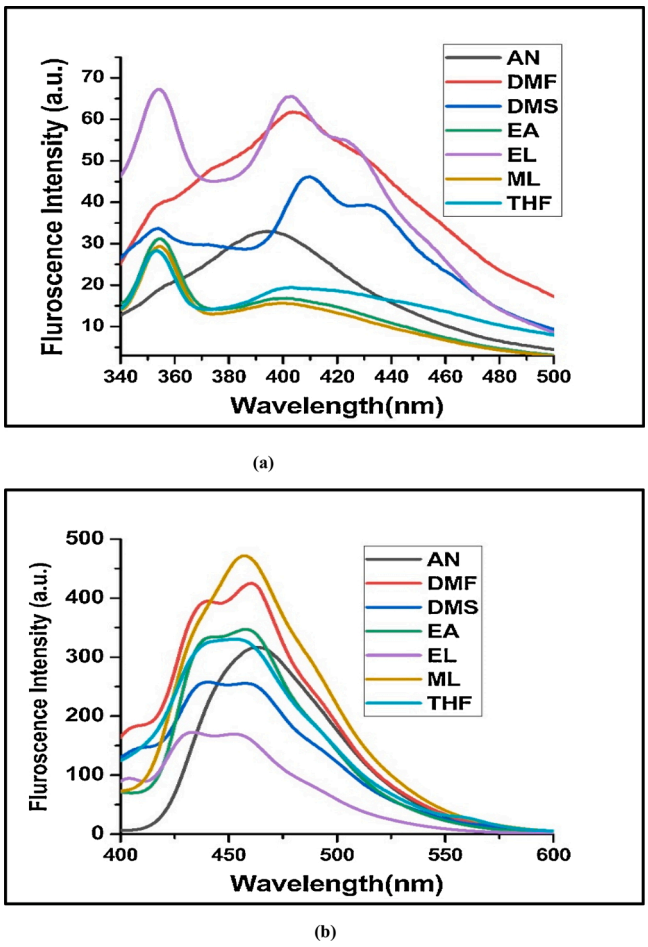

Fig. 5. Typical emission spectra for (a) 3OCE and (b) 3OBC in different solvents.

where $\Delta\mu_b = 9D$ and a_B =6.2 Å are the change in dipole moment after excitation and it is determined by the following Eq. (15) as given below

$$\Delta\mu = \left(\mu_e-\mu_g\right) = \sqrt{\frac{(m\ x\ 81)}{\left(\frac{6.2}{a}\right)^3\ x\ 11307.6}} \quad (15)$$

Where 'm' is the slope of the linear plot of Stoke's shift versus E_T^N obtained from the linear fit of Eq. (14). The corresponding plots stokes shift $\left(\overline{\nu}_a-\overline{\nu}_f\right)$ against E_T^N, obtained from the relation (14) is shown in Fig. 9 (a),(b) for 3OCE and 3OBC compounds respectively. It is observed that, the increment in value of dipole moments in excited states is attributed to specific effect of solvent likely hydrogen bonding effect and complex formation etc. The difference in μ_e values for variety of solutes may be because of their structural differences [54 and 55]

From the Table 5 we can say that, the μ_e values are found to be more for 3OCE and and less for 3OBC compounds as compared to other models. This is due to the fact that, this model considers the specific solvent-solute interactions [29].

3.2. Quantum chemical calculations

3.2.1. Theoretical approach for evaluating ground and excited state dipole moments

Theoretically dipole moment at the ground state for 3OCE and 3OBC compounds is determined using DFT/B3LYP method with basis set of 6−311++G (d, p) [45–50] which is calculated as 4.566D for 3OCE and 5.270D for 3OBC compounds. The optimized geometry in ground state

Table 1
Photo physical parameters of 3OCE in different solvents.

Solvents	$\lambda_a(nm)$	$\lambda_e(nm)$	$\bar{\nu}_a(cm^{-1})$	$\bar{\nu}_f(cm^{-1})$	$(\bar{\nu}_a - \bar{\nu}_f)$ (cm^{-1})	$(\bar{\nu}_a + \bar{\nu}_f)/2$ (cm^{-1})
ML	360	465.00	27777.78	21505.38	6272.40	24641.58
AN	355	457.00	28169.01	21881.84	6287.18	25025.43
EL	362	454.00	27624.31	22026.43	5597.88	24825.37
DMF	338	407.00	29585.80	24570.02	5015.77	27077.91
DMS	340	408.00	29411.76	24509.80	4901.96	26960.78
THF	362	420.00	27624.31	23809.52	3814.79	25716.92
EA	357	402.00	28011.20	24875.62	3135.58	26443.41

Table 2
Photo physical parameters of 3OBC in different solvents.

Solvents	$\lambda_a(nm)$	$\lambda_e(nm)$	$\bar{\nu}_a(cm^{-1})$	$\bar{\nu}_f(cm^{-1})$	$(\bar{\nu}_a - \bar{\nu}_f)$ (cm^{-1})	$(\bar{\nu}_a + \bar{\nu}_f)/2$ (cm^{-1})
ML	411.00	465.00	24330.90	21505.38	2825.52	22918.14
AN	415.00	467.00	24096.39	21413.28	2683.11	22754.83
EL	414.00	466.00	24154.59	21459.23	2695.36	22806.91
DMF	416.00	464.00	24038.46	21551.72	2486.74	22795.09
DMS	415.00	462.00	24096.39	21645.02	2451.36	22870.70
THF	416.00	461.00	24038.46	21691.97	2346.49	22865.22
EA	415.00	461.00	24096.39	21691.97	2404.41	22894.18

Table 3
Dielectric constant (ε), refractive index (*n*), solvent polarity functions, Microscopic solvent polarity parameter (E_T^N) for 3OCE and 3OBC.

Solvents	ε	*n*	$F_1(\varepsilon,n)$	$F_2(\varepsilon,n)$	$F_3(\varepsilon,n)$	E_N^T
ML	33.7	1.328	0.309	0.858	0.652	0.762
AN	37.5	1.346	0.305	0.863	0.667	0.46
EL	24.35	1.361	0.289	0.812	0.652	0.654
DMF	38.25	1.43	0.275	0.839	0.711	0.404
DMS	47.24	1.479	0.263	0.841	0.744	0.444
THF	7.58	1.407	0.210	0.549	0.551	0.207
EA	6.08	1.372	0.201	0.493	0.499	0.228

for 3OCE and 3OBC is shown in Fig. 10 (a),(b). The direction of dipole moment is represented by direction of the arrow head. On comparing the experimental and theoretical dipole moments in ground state, a huge discrepancy was found. However, the existence of such discrepancy might be as a consequence of consideration of gas phase and also a possibility due to exclusion of interaction between solute and solvent through the theoretical approach.

3.2.2. *Analyzing the frontier molecular orbital*

Frontier molecular orbital analysis is done using computational Chemistry for determining number of active sites, chemical reactivity and kinetic stability of the molecules. HOMO represents ability to loose electrons and LUMO represents ability to gain electrons for the heterocyclic compounds. Charge transfer properties of heterocyclic compounds is studied through this analysis. The analysis [20] uses DFT/B3LYP with basic set 6−311++G (d, p). The Fig. 11(a) and (b) shows HOMO-LUMO three dimensional plots of 3OCE and 3OBC molecules respectively.

Small energy gap corresponds to a soft molecule indicating that the compounds are more reactive where large energy gap corresponds to hard molecule and molecular stability of the measurer. Koopmans' theorem states ionization potential (IP) and electron affinity (EA) as EA = $-E_{LUMO}$ and IP= $-E_{HOMO}$ [57]. We use χ =[(IP + EA)/2] to determine Electronegativity (χ) and V=-[(IP + EA)/2] to calculate chemical potential (V) [20]. Chemical reactivity is determined through chemical softness (S) and chemical stability is measured by chemical hardness. Chemical softness is given as inverse of chemical hardness (i.e $S=\frac{1}{\eta}$) and chemical hardness (η) is given as η= [(IP-EA)/2] [34,43].The relation, $\omega = \frac{\mu^2}{2\eta}$ is used for determining the eletrophilicity index which informs

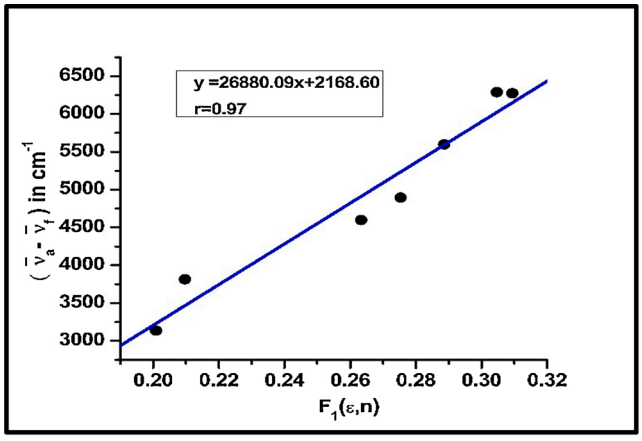

(a) 3OCE

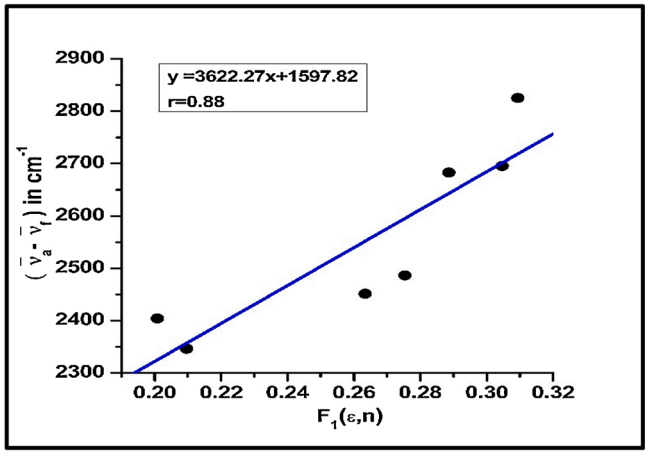

(b) 3OBC

Fig. 6. The variation of Stoke's shift with F_1 (ε, n) using Lippert equation for 6 (a)3OCE and 6(b)3OBC.

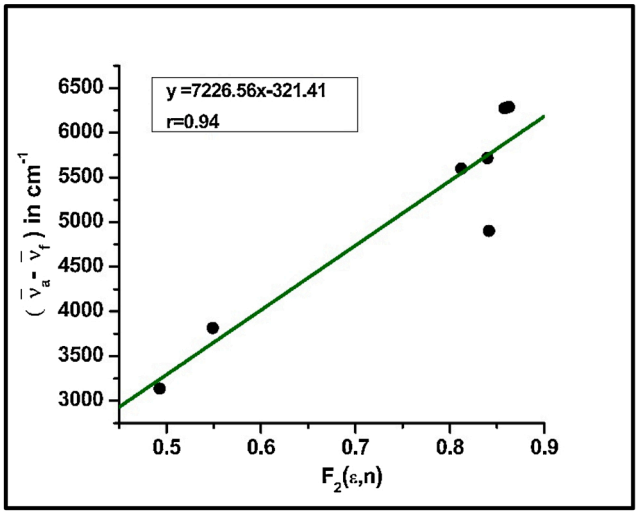

(a) 3OCE

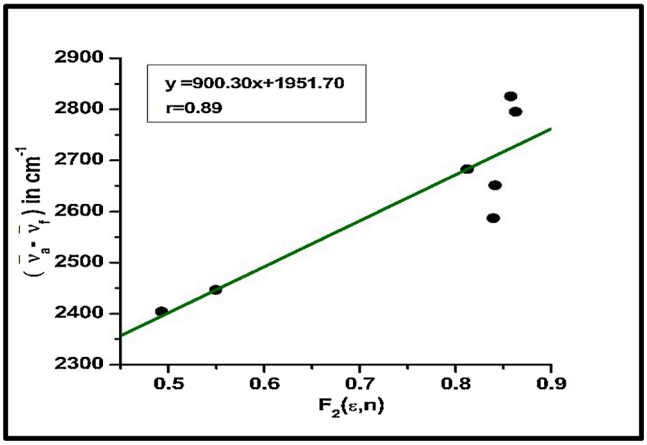

(b) 3OBC

Fig. 7. The variation of Stoke's shift with F_2 (ε, n) using Bakshiev's equation for 7(a) 3OCE and 7(b) 3OBC.

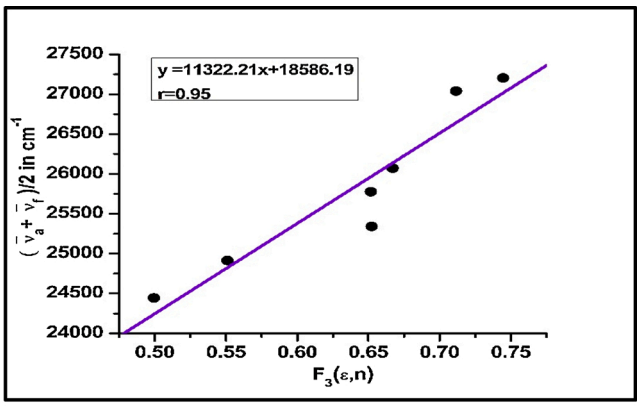

(a) 3OCE

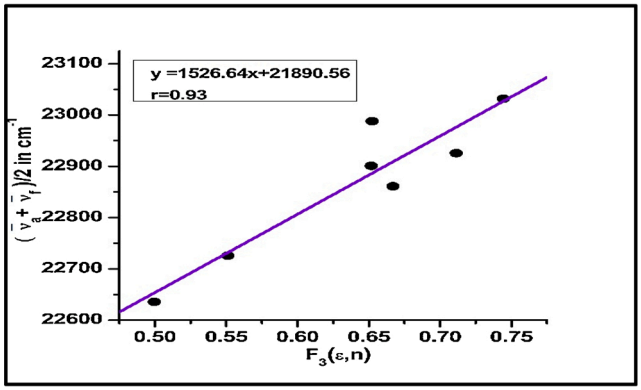

(b) 3OBC

Fig. 8. The variation of arithmetic means of Stoke's shift with F_3 (ε, n) using Kawski- Chamma-Viallet's equation for 8(a) 3OCE and 8(b) 3OBC.

about the electrophilic property of a compound [20]. Table 6 shows the determined frontier molecular orbital and the related molecular properties for 3OCE and 3OBC compounds. The energy gap for 3OCE is observed to be 2.995 eV and 2.966 eV for 3OBC. There is a possibility of nucleophilic and electrophilic attack which is indicated by low values of electron affinity and higher values of ionization potential for 3OCE and 3OBC compounds [34].

3.2.3. Molecular Electrostatic Potentials (MEP) and analysis of contour map

Molecular electrostatic potentials (MEPs) is the cloud of charged particles that surround molecules.The nucleophilic and electrophilic property for the molecules is identified by colored regions shown.

Table 4
Statistical treatment of the correlations of solvents spectral shifts of 3OCEand 3OBC.

Compounds	Method	Slope	Intercept	Correlation factor 'r'	Number of data (N)
3OCE	Lippert Correlation	26880.09	2468.60	0.97	7
	Bakhshiev's Correlation	7226.56	−321.41	0.94	7
	Kawaski-Chamma-Viallet Correlation	11322.21	18586.19	0.95	7
	Reichards Correlation	5072.86	2512.75	0.93	7
3OBC	Lippert Correlation	3622.27	1597.82	0.88	7
	Bakhshiev's Correlation	900.30	1951.70	0.89	7
	Kawaski-Chamma-Viallet Correlation	1526.64	21890.56	0.93	7
	Reichards Correlation	180.50	2575.39	0.91	7

Table 5
Ground state and excited state dipole moments of 3OCE and 3OBC.

Compound	Radius 'a'(A^0)	μ_g[a] (D)	μ_g[b](D)	μ_e[c](D)	μ_e[d](D)	μ_e[e](D)	μ_e[f](D)	μ_e[g](D)	$\Delta\mu$[h]	$\Delta\mu$[i]	$\left(\frac{\mu_e}{\mu_g}\right)$[j]	Φ[k]
3OCE	3.994	4.566	1.917	8.681	14.963	8.681	8.681	5.034	6.764	3.117	4.529	0°
3OBC	4.202	5.271	0.896	3.473	6.064	3.473	3.473	1.531	2.576	0.634	3.875	0°

Debye (D) = 3.33564 × 10–30 cm = 10^{-18}esu cm.
*j*The ratio of excited state and ground state dipole moment.
[k]The angle between ground state and excited state dipole moments calculated using Eq.(13).
[a] The ground states dipole moments calculated using Gaussian software.
[b] The ground states dipole moments calculated using Eq.(7).
[c] The excited states dipole moments calculated using Eq.(8).
[d] The experimental excited states dipole moments calculated from Lippert's equation.
[e] The experimental excited states dipole moments calculated from Bakshiev's equation.
[f] The experimental excited states dipole moments calculated from Kawaski-Chamma-Viallet equation.
[g] The excited states dipole moments calculated from E_N^T equation.
[h] The change in dipole moments for μ_e and μ_g.
[i] The change in dipole moments calculated from Eq.(16).

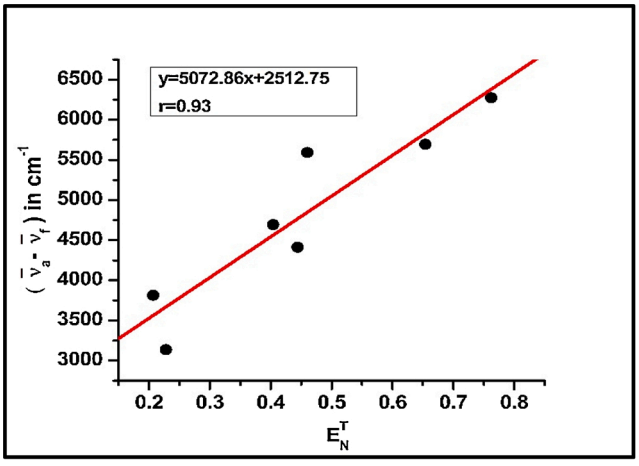

(a) 3OCE

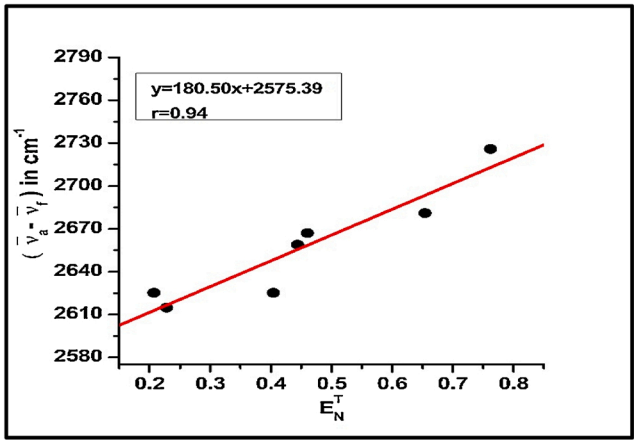

(b) 3OBC

Fig. 9. The variation of Stoke's shift with E_T^N for 9(a) 3OCE and 9(b) 3OBC.

Electrostatic potentials, V(r), of the molecules can be given by Eqn. (16) [34]

$$V(r) = \sum\left[\frac{Z_R}{|R_A - r|}\right] - \int\left[\frac{\rho(r')dr'}{|r' - r|}\right] \quad (16)$$

where,

Z_R - charge of nucleus A located at R_A
$\rho(r')$ - represents the solute's electron density function
r' - refers to the dummy's integration variable

Contour maps for 3OCE and 3OBC compounds is shown in Fig. 12 (a) and (b). Electrophilic (electron rich) reactivity is represented by the dark red colored region surrounding the oxygen atom and nucleophilic (electron deficient) reactivity is shown by the dark blue colored region surrounding the hydrogen atom of 3OCE and 3OBC compounds. It is observed that, color code of MEP diagram lies between -0.0594 a. u (Dark red) and 0.0594 a. u. (Dark blue) for 3OCE compound and -0.06118 a. u (Dark red) and 0.06118 a. u (Dark blue) for 3OBC compound. Fig. 13(a) and (b) shows the contour map for molecular electrostatic potential surface of 3OCE and 3OBC compounds. In addition, it confirms for the positive and negative regions of the molecules in agreement with total electron density surface. Available sites for nucleophilic and electrophilic reaction is shown by MEP as well as contour analysis.

3.2.4. *Evaluating atomic charges*

The concept of charge transfer and atomic charges is used in explanation of reactivity and molecular behavior in quantum chemistry. B3LYP methods with basis level of 6−311++G (d, p) in Mulliken population study is used for evaluating the atomic charge number on each atom the compounds under investigation [20]. Mulliken charge distribution for 3OCE and 3OBC compounds is shown in Fig. 14 (a) and (b). Table 7(a) and (b) lists down the Mulliken atomic charge distribution for both the compounds. A total 35 atoms for 3OCE and 41 atoms for 3OBC are present.

3.2.5. *Fukui function analysis*

In heterocyclic compounds, Fukui function is used mostly for reactive indicators. The representation of Fukui function is given by Eqn. (17)

$$F(r) = \frac{\partial\rho(r)}{\partial N} \quad (17)$$

where,

r is the external potential exerted by nucleus
N refers to the number of electrons
ρ(r) represents the electronic density

Upon accepting or donating electrons in heterocyclic molecules, the identification of electron density and reactive sites at given position is done by Fukui [56–62].

Given below is the definition for possible atomic Fukui functions on jth atom site:

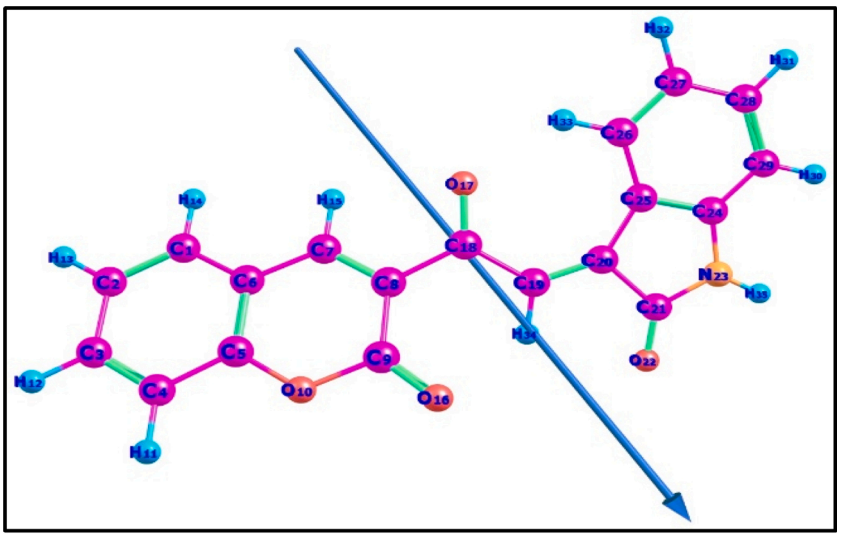

(a) 3OCE

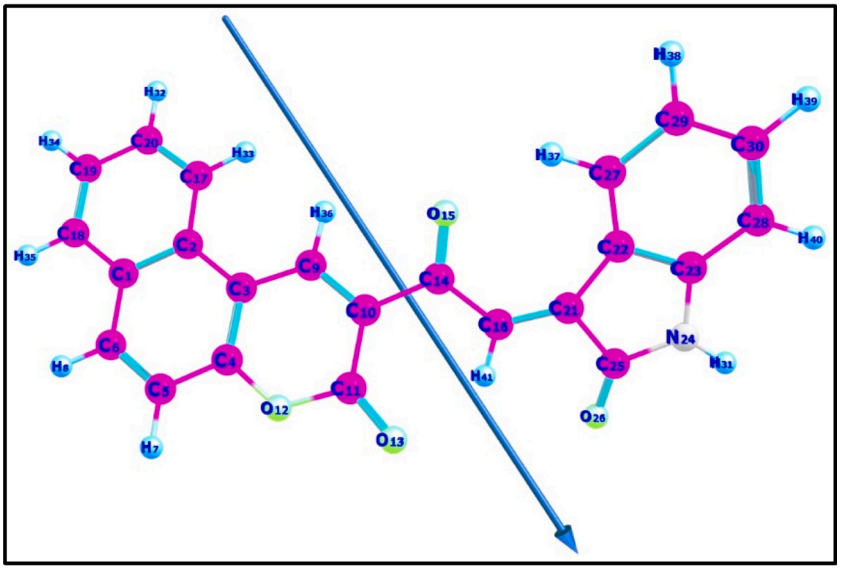

(b) 3OBC

Fig. 10. Ground state optimized molecular geometries of 10 (a) 3OCE and 10 (b) 3OBC. The arrow indicates the direction of the dipole moment.

$$f_j^- = \left[q_j(N) - q_j(N-1)\right] \quad (18)$$

$$f_j^+ = \left[q_j(N+1) - q_j(N)\right] \quad (19)$$

$$f_j^0 = \left[q_j(N+1) - q_j(N-1)\right]/2 \quad (20)$$

$f_j^+(r)$ - nucleophilic Fukui function

$f_j^-(r)$ - electrophilic Fukui function

f_j^0 gives the Fukui function for free radical

qj represents the atomic charge at the jth atomic site

Eqn. (21) below shows calculation of Fukui function as an intramolecular reactivity index [56–63] from NBO charges

$$\int f(r)dr = 1 \quad (21)$$

In this study, calculations are performed using ground state with double multiplicity at DFT/B3LYP 6−311++G (d, p) basis set for single point energy in the anionic and cationic form of the 3OCE and 3OBC

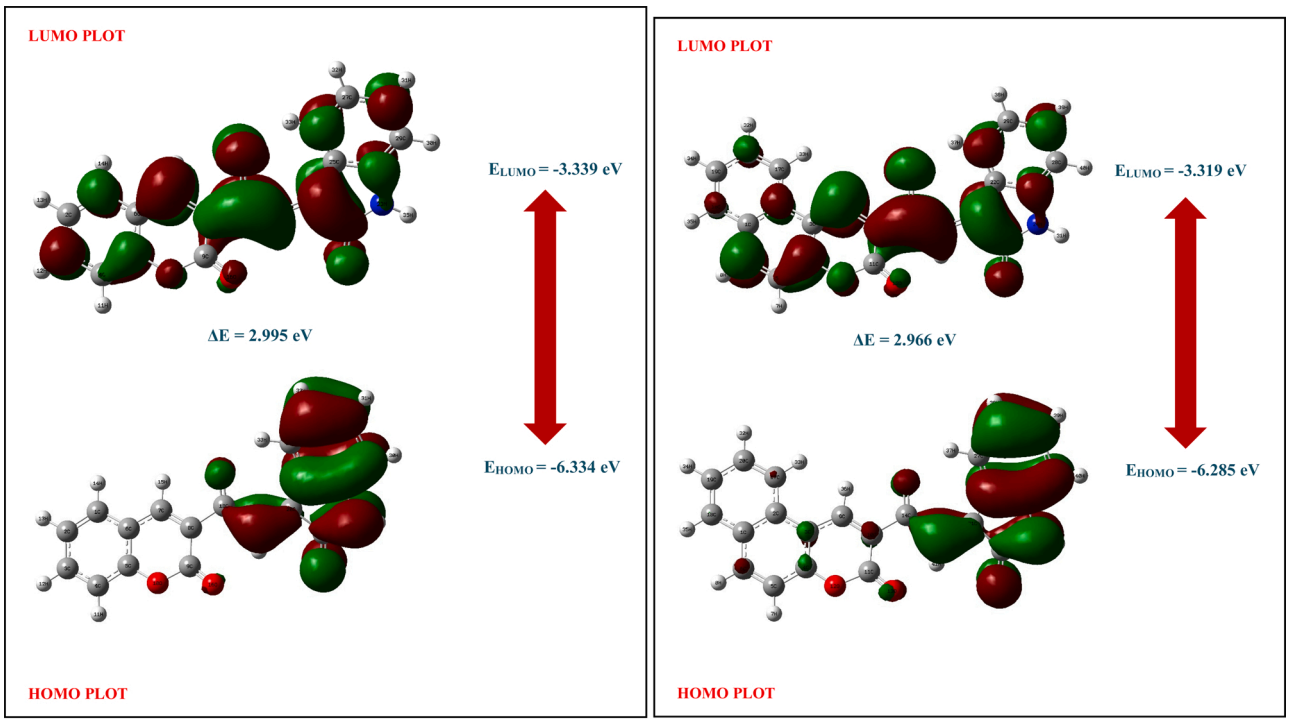

Fig. 11. HOMO-LUMO Structure of 11 (a) 3OCE and 11 (b) 3OBC.

Table 6
The calculated FMOs and related molecular properties values of the 3OCE and 3OBC.

Molecular properties	Energy (in eV) for 3OCE	Energy (in eV) for 3OBC
HOMO	−6.334	−6.285
LUMO	−3.339	−3.319
E_{HOMO}-E_{LUMO}	2.995	2.966
Ionization potential (IP)	6.334	6.285
Electron affinity(EA)	3.339	3.319
Electronegativity(χ)	4.837	4.802
Hardness(η)	1.498	1.483
Softness(S)	0.668	0.674
Chemical potential(μ)	−4.837	−4.802
Electrophilicity index(ω)	7.811	7.776

compounds. Table 8(a) and (b) shows the determined values of local reactivity descriptors such as Fukui functions (f_k^+, f_k^-, f_k°), local electrophilicity indices (ω_k^+, ω_k^-, ω_k°) and local softness (S_k^+, S_k^-, S_k°). These descriptors are based on electron density. For 3OCE, most of the nucleophilic reactive atoms were observed to follow the order of O22 > C27 > N23 > H32. Atoms C27 and H32 are identified to be high reactive site for a nucleophilic attack and are also present in benzene ring. In the case of 3OBC, electrophilic reactive atoms are found to follow C20 > O17 > C7 > H31 order. Atoms C20, O17 and H31 are highly reactive site for an electrophilic attack and are found to be present in the benzene. However O22, C20, C27 and H31 atoms are identified to be favorable sites for radical attack. In Table 8 (b), it is clearly shown that for 3OBC, atoms C29, H38 and H39 are identified as reactive region being present in the benzene ring for nucleophilic attack and atoms C9, C10, C6 and H8 for electrophilic attack being identified as reactive region. And atoms C21, O26, O15 andC9 are favorable sites for the radical attack.

3.2.6. Analysis of natural bonding orbital (NBO)

The analysis of natural bonding orbital (NBO) provides an important inter and intra molecular bonding for identifying hyper-conjugative interactions or charge transfer probability [48,49]. NBO 5.0 software is used for studying re-hybridization of 3OCE and 3OBC. Also Gaussian 9 W software is used for determining delocalization of electron density and intra-molecular charge distribution inside the molecule. Bonding and anti-bonding interactions are analyzed through NBO analysis in a qualitative way. The perturbation energies E(2) is given by the Eqn. (22) [41–44].

$$E(2) = \Delta Eij = qi\frac{F^2_{(ij)}}{(E_i - E_j)} \quad (22)$$

Where

$F_{(ij)}$ shows off-diagonal matrix element for NBO Fock matrix element

q_i represents the occupancy of donor orbital

E_i and Ej are the energies of diagonal elements,

Various parameters of NBO basis for both the compounds is depicted in both the compounds. Table 9(a) and (b). Two donors and two acceptors are observed to be available for different perturbation energy transitions such as C21- N23 → C27-C28 (395.09 kj/mol, π→π*), N23-C24 →C8-C9 (311.66kj/mol, π→π*), N23-H35→ C8-C9 (606.52kj/mol, π →π*) and for 3OBC, C22-C27 → C23-C28 (24.05kj/mol, π→π*), C29-C30→C22-C27 (23.15kj/mol, π→π*), C5-C6→C3-C4 (21.32kj/mol, π→π*) are the most probable transitions for 3OCE. From these transitions we can say that transitions happen only within phenyl ring and major contribution is by π electrons which are having Intramolecular hyper conjugative interactions. However in case of 3OBC molecule, transition takes place from the lone pair of O13 to σ*(C11-O12) and O12 to σ*(C11-O13) which is responsible for the stabilization of the system. Further, π →π* transition is responsible for the NLO activity of 3OCE and 3OBC compounds.

3.2.7. Analysis of molecular docking

The molecular docking for both compounds 3OCE and 3OBC were carried out using AutoDock. The crystal structure of galactose binding

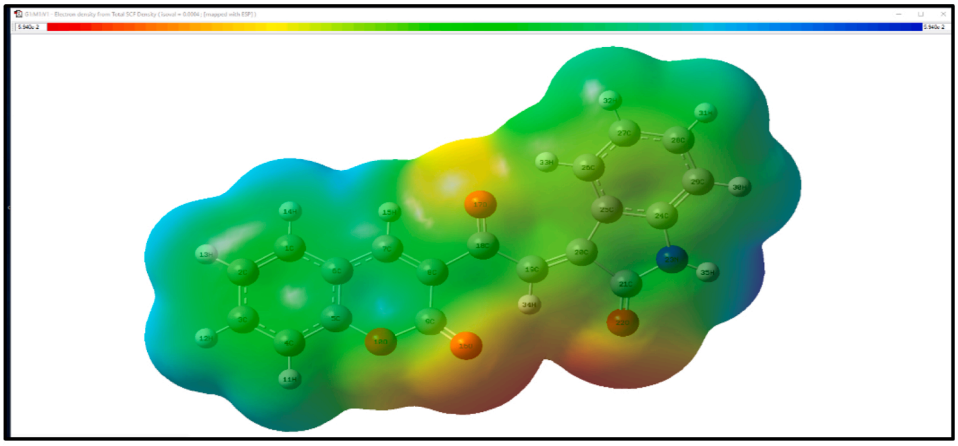

(a) 3OCE

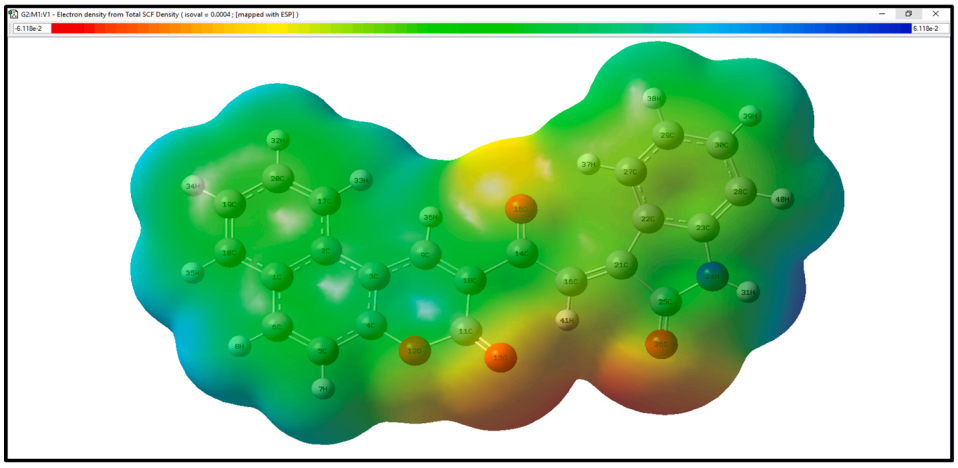

(b) 3OBC

Fig. 12. The total electron density mapped with the MEP surface for 12 (a) 3OCE and 12 (b) 3OBC.

periplasmic protein (PDB ID: 2IPM and 2IPL) was retrieved from protein data bank, pre-processing and preparation of the protein for docking was performed by using VMD 1.9.3. The molecular docking for both compounds 3OCE and 3OBC were carried out using Auto Dock Tools version 1.5.6 software. The binding affinity mode of docked compound 3OCE and 3OBC with 2-IPM and IPL are as shown in Fig. 2(a) & (b) and Fig. 3 (a) & (b) respectively. Interaction of 2IPM and 2IPL protein for both compounds 3OCE and 3OBC with docked energy parameters as shown Table 10. These parameters infer that the coumarin compounds will bind strongly with periplasmic proteins of the blood [64,65].

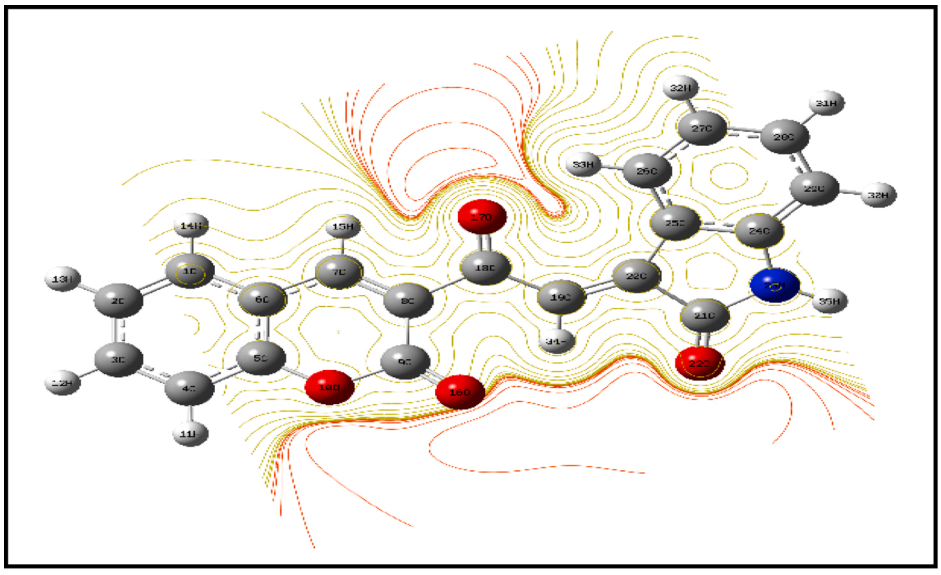

(a) 3OCE

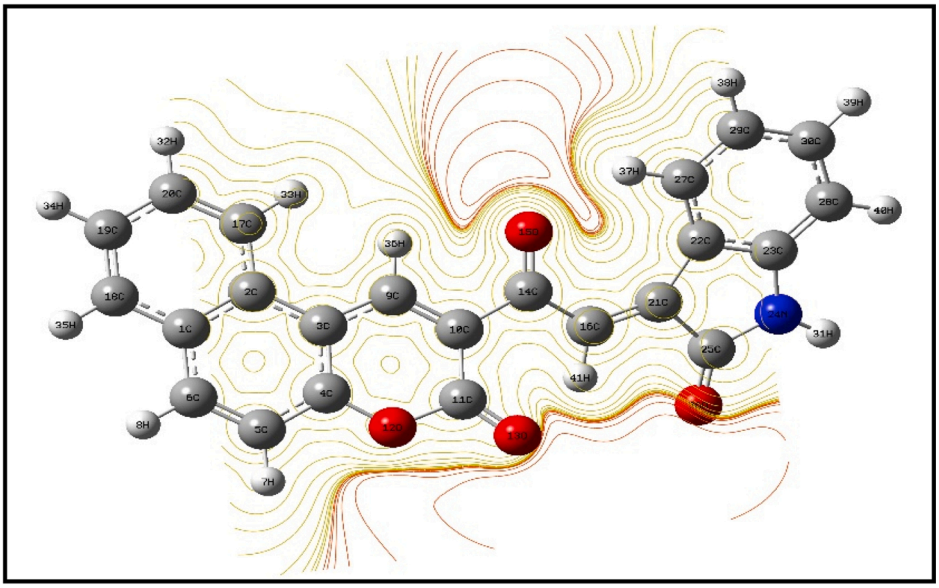

(b) 3OBC

Fig. 13. The contour map of molecular electrostatic potential surface for 13 (a) 3OCE and 13 (b) 3OBC.

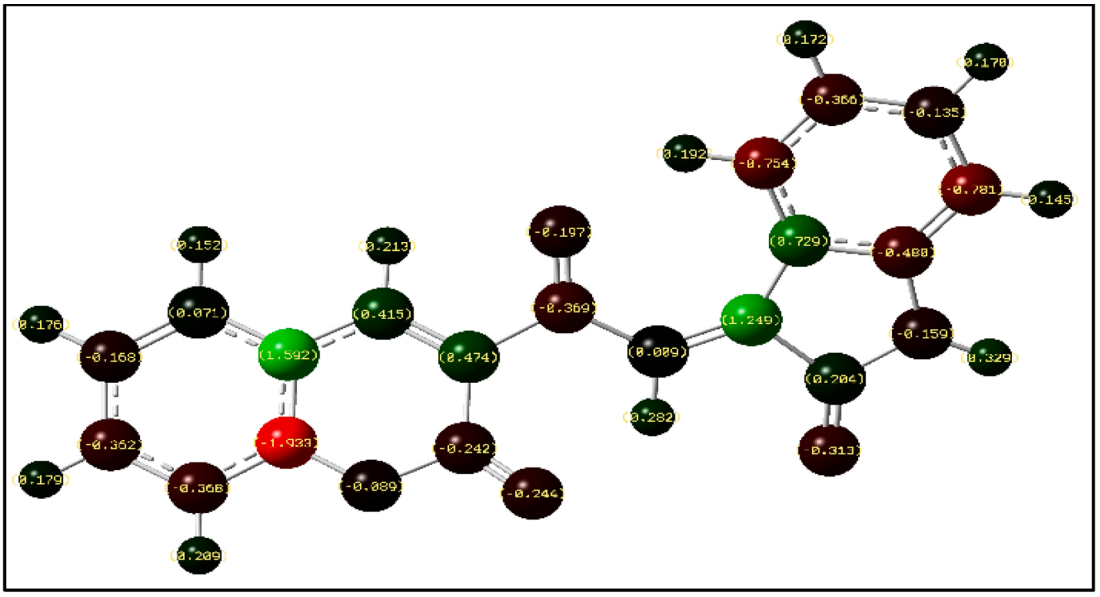

(a) 3OCE

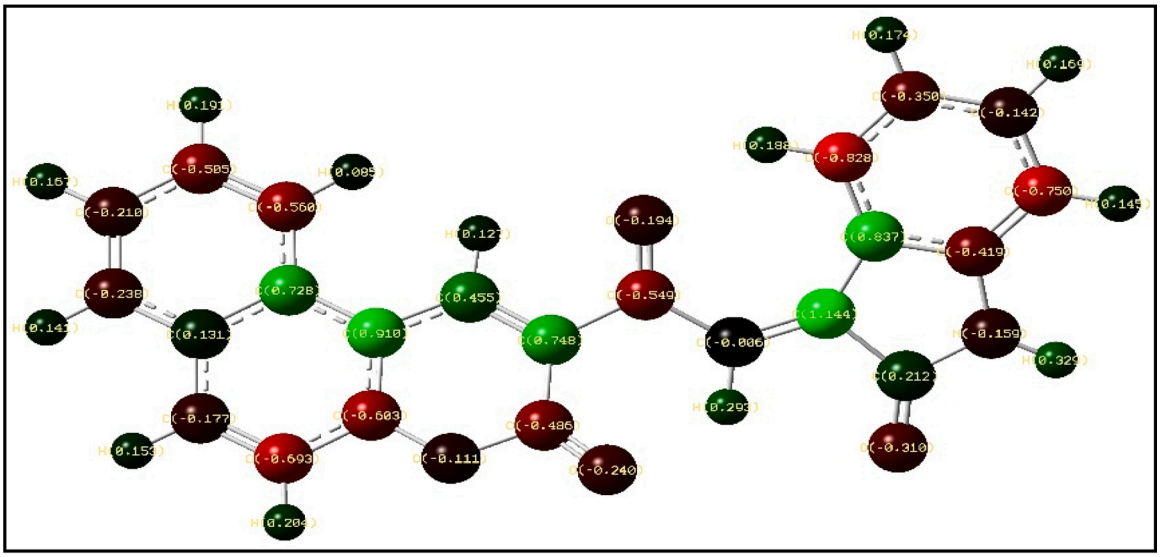

(b) 3OBC

Fig. 14. Mulliken charges for 14 (a) 3OCE and 14 (b) 3OBC.

Table 7
(a) Calculated Mulliken atomic charge distribution of 3OCE.

Atoms	Mulliken atomic charge distribution		
	Anion q(N-1)	Neutral q(N)	Cation q(N + 1)
C1	0.0294	0.0711	0.0961
C2	−0.1769	−0.1681	−0.1465
C3	−0.3983	−0.3620	−0.3501
C4	−0.3760	−0.3673	−0.3577
C5	−1.9284	−1.9324	−1.9422
C6	1.6064	1.5913	1.6085
C7	0.3565	0.4139	0.4314
C8	0.4281	0.4740	0.4954
C9	−0.2097	−0.2423	−0.2450
O10	−0.1217	−0.0893	−0.0603
H11	0.1743	0.2094	0.2349
H12	0.1347	0.1789	0.2133
H13	0.1364	0.1760	0.2094
H14	0.1228	0.1515	0.1722
H15	0.1827	0.2127	0.2298
O16	−0.2823	−0.2443	−0.2156
O17	−0.2932	−0.1973	−0.1709
C18	−0.4105	−0.3696	−0.3780
C19	−0.0135	0.0098	0.0664
C20	1.1294	1.2504	1.3032
C21	0.1840	0.2044	0.1962
O22	−0.3858	−0.3126	−0.2105
N23	−0.1702	−0.1586	−0.0942
C24	−0.4507	−0.4817	−0.4868
C25	0.7331	0.7305	0.7709
C26	−0.7623	−0.7552	−0.7520
C27	−0.3993	−0.3668	−0.2952
C28	−0.1714	−0.1348	−0.1109
C29	−0.7849	−0.7819	−0.7669
H30	0.1066	0.1452	0.1971
H31	0.1252	0.1700	0.2289
H32	0.1362	0.1722	0.2340
H33	0.1948	0.1922	0.2197
H34	0.2598	0.2817	0.2996
H35	0.2948	0.3288	0.3758

(b) The calculated Mulliken atomic charge distribution of 3OBC.

Atoms	Mulliken atomic charge distribution		
	Anion q(N-1)	Neutral q(N)	Cation q(N + 1)
C1	0.1555	0.1314	0.1158
C2	0.6997	0.7276	0.7250
C3	0.9015	0.9100	0.9515
C4	−0.6212	−0.6032	−0.6001
C5	−0.6856	−0.6925	−0.6912
C6	−0.2253	−0.1775	−0.1454
H7	0.1695	0.2037	0.2337
H8	0.1099	0.1527	0.1890
C9	0.3783	0.4548	0.4732
C10	0.6992	0.7482	0.7851
C11	−0.4522	−0.4860	−0.4951
O12	−0.1450	−0.1111	−0.0821
O13	−0.2778	−0.2398	−0.1955
C14	−0.5688	−0.5490	−0.5579
O15	−0.2838	−0.1942	−0.1733
C16	−0.0271	−0.0062	0.0328
C17	−0.5486	−0.5598	−0.5350
C18	−0.2594	−0.2378	−0.2007
C19	−0.2159	−0.2097	−0.1947
C20	−0.5252	−0.5053	−0.4933
C21	1.0317	1.1437	1.1885
C22	0.8424	0.8367	0.8647
C23	−0.3938	−0.4188	−0.4224
N24	−0.1697	−0.1593	−0.1128
C25	0.1927	0.2121	0.2103
O26	−0.3776	−0.3103	−0.2319
C27	−0.8352	−0.8277	−0.8264
C28	−0.7549	−0.7502	−0.7371
C29	−0.3814	−0.3505	−0.2949
C30	−0.1743	−0.1421	−0.1224
H31	0.2979	0.3293	0.3670
H32	0.1623	0.1913	0.2225
H33	0.0842	0.0850	0.1031

Table 7 (*continued*)

(b) The calculated Mulliken atomic charge distribution of 3OBC.

Atoms	Mulliken atomic charge distribution		
	Anion q(N-1)	Neutral q(N)	Cation q(N + 1)
H34	0.1341	0.1672	0.2039
H35	0.1125	0.1412	0.1758
H36	0.1078	0.1268	0.1372
H37	0.1919	0.1881	0.2055
H38	0.1410	0.1737	0.2212
H39	0.1277	0.1693	0.2171
H40	0.1093	0.1452	0.1874
H41	0.2740	0.2925	0.3020

4. Conclusions

The results and discussions obtained from the study of 3OCE and 3OBC coumarin compounds infers the following points:

(1) For both the compounds, polar nature in excited state is more as compared to ground state as indicate by large value of dipole moment in excited state.
(2) Observing the Red shift for both 3OCE and 3OBC compounds confirms $\pi \rightarrow \pi^*$ and ICT character.
(3) Low energy gap values between HOMO-LUMO signifies high molecular reactivity for both the compounds 3OCE and 3OBC.
(4) The intra-molecular interactions of both compounds are confirmed by NBO analysis.
(5) Electrophilic and nucleophilic reactive sites are predicted in case of both compounds.
(6) The local softness and local electrophilicity indices of 3OCE and 3OBC are determined by Fukui functions.
(7) Molecular docking study revealed that both the coumarin compounds 3OCE and 3OBC showed best suitable binding pattern at the active site by interacting non-covalently with amino acid residues of proteins.

Author contribution statements

Raveendra Melavanki: Experimental part corrections and manuscript preparation.

Kalpana Sharma: Theoretical part corrections and manuscript preparation.

V. T. Muttannavar: Experimental part did.

Raviraj Kusanur: Involved in experimental work and calculations.

Kariyappa Katagi: Theoretical part did.

Swarna M Patra: Involved in theoretical calculations.

Siva Umapathy: Theoretical part facility providing and guiding for work from lab.

Kishor Kumar Sadasivuni: Molecular docking work carried out.

Vikas M Shelar: Some experimental work did.

Diksha Singh: Some experimental work did.

N R Patil: Some Theoretical part calculations did.

V V Koppal: Some theoretical calculations did.

Declaration of Competing Interest

This to certify that the article entitled “Quantum chemical computations, Fluorescence spectral features and molecular docking of two biologically active heterocyclic class of compounds” submitted by Raveendra Melavanki etal for the publication in Journal of Photochemistry and Photobiology A: Chemistry is based on the original work and results of the experiments are carried out by all authors under my supervision. No part of the article has been previously submitted for the publication in any journals.

Table 8

(a) The calculated Fukui functions, local softness and local eletrophilicity indices of 3OCE.

Atoms	f_k^+	f_k^-	f_k^0	S_k^+	S_k^-	S_k^0	ω_k^+	ω_k^-	ω_k^0
C1	0.0250	0.0417	0.0334	0.0167	0.0279	0.0223	0.1952	0.3260	0.2606
C2	0.0216	0.0089	0.0152	0.0144	0.0059	0.0102	0.1685	0.0692	0.1188
C3	0.0119	0.0363	0.0241	0.0079	0.0242	0.0161	0.0926	0.2834	0.1880
C4	0.0096	0.0087	0.0092	0.0064	0.0058	0.0061	0.0752	0.0683	0.0717
C5	−0.0098	−0.0040	−0.0069	−0.0065	−0.0027	−0.0046	−0.0765	−0.0312	−0.0538
C6	0.0172	−0.0150	0.0011	0.0115	−0.0101	0.0007	0.1342	−0.1175	0.0083
C7	0.0175	0.0574	0.0375	0.0117	0.0383	0.0250	0.1370	0.4482	0.2926
C8	0.0214	0.0459	0.0336	0.0143	0.0307	0.0225	0.1670	0.3587	0.2628
C9	−0.0027	−0.0326	−0.0176	−0.0018	−0.0218	−0.0118	−0.0208	−0.2545	−0.1376
O10	0.0290	0.0324	0.0307	0.0194	0.0217	0.0205	0.2267	0.2532	0.2400
H11	0.0255	0.0350	0.0303	0.0170	0.0234	0.0202	0.1992	0.2736	0.2364
H12	0.0344	0.0442	0.0393	0.0230	0.0295	0.0263	0.2688	0.3455	0.3072
H13	0.0334	0.0396	0.0365	0.0223	0.0264	0.0244	0.2605	0.3091	0.2848
H14	0.0207	0.0287	0.0247	0.0138	0.0192	0.0165	0.1617	0.2244	0.1930
H15	0.0171	0.0300	0.0235	0.0114	0.0200	0.0157	0.1335	0.2341	0.1838
O16	0.0287	0.0380	0.0334	0.0191	0.0254	0.0223	0.2239	0.2971	0.2605
O17	0.0264	0.0959	0.0612	0.0176	0.0641	0.0409	0.2060	0.7494	0.4777
C18	−0.0084	0.0409	0.0163	−0.0056	0.0273	0.0109	−0.0654	0.3193	0.1270
C19	0.0566	0.0233	0.0399	0.0378	0.0156	0.0267	0.4418	0.1819	0.3119
C20	0.0529	0.1210	0.0869	0.0353	0.0808	0.0581	0.4129	0.9452	0.6790
C21	−0.0082	0.0204	0.0061	−0.0055	0.0136	0.0041	−0.0642	0.1594	0.0476
O22	0.1021	0.0733	0.0877	0.0682	0.0489	0.0586	0.7973	0.5724	0.6848
N23	0.0644	0.0116	0.0380	0.0430	0.0078	0.0254	0.5030	0.0908	0.2969
C24	−0.0051	−0.0310	−0.0181	−0.0034	−0.0207	−0.0121	−0.0396	−0.2425	−0.1410
C25	0.0404	−0.0026	0.0189	0.0270	−0.0018	0.0126	0.3156	−0.0206	0.1475
C26	0.0031	0.0071	0.0051	0.0021	0.0048	0.0034	0.0245	0.0558	0.0401
C27	0.0717	0.0325	0.0521	0.0479	0.0217	0.0348	0.5598	0.2535	0.4066
C28	0.0239	0.0366	0.0303	0.0159	0.0245	0.0202	0.1865	0.2861	0.2363
C29	0.0149	0.0030	0.0090	0.0100	0.0020	0.0060	0.1166	0.0233	0.0700
H30	0.0519	0.0386	0.0452	0.0347	0.0258	0.0302	0.4053	0.3013	0.3533
H31	0.0589	0.0449	0.0519	0.0394	0.0300	0.0347	0.4603	0.3503	0.4053
H32	0.0617	0.0360	0.0489	0.0412	0.0241	0.0327	0.4823	0.2815	0.3819
H33	0.0275	−0.0026	0.0124	0.0183	−0.0017	0.0083	0.2145	−0.0202	0.0972
H34	0.0179	0.0219	0.0199	0.0120	0.0147	0.0133	0.1398	0.1713	0.1556
H35	0.0470	0.0340	0.0405	0.0314	0.0227	0.0270	0.3673	0.2652	0.3162

(b) The calculated Fukui functions, local softness and local eletrophilicity indices of 3OBC.

Atoms	f_k^+	f_k^-	f_k^0	S_k^+	S_k^-	S_k^0	ω_k^+	ω_k^-	ω_k^0
C1	−0.0156	−0.0241	−0.0198	−0.0105	−0.0162	−0.0134	−0.1213	−0.1870	−0.1542
C2	−0.0026	0.0279	0.0126	−0.0018	0.0188	0.0085	−0.0204	0.2167	0.0981
C3	0.0414	0.0085	0.0250	0.0279	0.0057	0.0168	0.3221	0.0663	0.1942
C4	0.0032	0.0180	0.0106	0.0021	0.0121	0.0071	0.0247	0.1399	0.0823
C5	0.0013	−0.0069	−0.0028	0.0009	−0.0047	−0.0019	0.0104	−0.0539	−0.0217
C6	0.0321	0.0478	0.0399	0.0216	0.0322	0.0269	0.2495	0.3717	0.3106
H7	0.0300	0.0342	0.0321	0.0202	0.0231	0.0216	0.2332	0.2660	0.2496
H8	0.0363	0.0429	0.0396	0.0245	0.0289	0.0267	0.2824	0.3334	0.3079
C9	0.0184	0.0765	0.0475	0.0124	0.0516	0.0320	0.1432	0.5948	0.3690
C10	0.0368	0.0491	0.0429	0.0248	0.0331	0.0289	0.2864	0.3815	0.3339
C11	−0.0092	−0.0338	−0.0215	−0.0062	−0.0228	−0.0145	−0.0712	−0.2626	−0.1669
O12	0.0290	0.0340	0.0315	0.0195	0.0229	0.0212	0.2255	0.2641	0.2448
O13	0.0443	0.0380	0.0412	0.0298	0.0256	0.0277	0.3442	0.2959	0.3201
C14	−0.0090	0.0198	0.0054	−0.0061	0.0134	0.0037	−0.0698	0.1543	0.0423
O15	0.0210	0.0896	0.0553	0.0141	0.0604	0.0373	0.1629	0.6971	0.4300
C16	0.0390	0.0209	0.0299	0.0263	0.0141	0.0202	0.3029	0.1626	0.2328
C17	0.0248	−0.0111	0.0068	0.0167	−0.0075	0.0046	0.1929	−0.0866	0.0531
C18	0.0371	0.0216	0.0293	0.0250	0.0145	0.0198	0.2884	0.1677	0.2281
C19	0.0149	0.0062	0.0106	0.0101	0.0042	0.0071	0.1162	0.0482	0.0822
C20	0.0120	0.0199	0.0159	0.0081	0.0134	0.0107	0.0933	0.1546	0.1239
C21	0.0448	0.1121	0.0784	0.0302	0.0755	0.0529	0.3485	0.8714	0.6099
C22	0.0279	−0.0057	0.0111	0.0188	−0.0038	0.0075	0.2171	−0.0440	0.0866
C23	−0.0036	−0.0249	−0.0143	−0.0025	−0.0168	−0.0096	−0.0283	−0.1937	−0.1110
N24	0.0465	0.0105	0.0285	0.0313	0.0070	0.0192	0.3613	0.0813	0.2213
C25	−0.0019	0.0194	0.0088	−0.0013	0.0131	0.0059	−0.0145	0.1512	0.0683
O26	0.0784	0.0673	0.0728	0.0528	0.0453	0.0491	0.6097	0.5230	0.5663
C27	0.0013	0.0076	0.0044	0.0008	0.0051	0.0030	0.0098	0.0588	0.0343
C28	0.0130	0.0047	0.0089	0.0088	0.0032	0.0060	0.1011	0.0368	0.0690
C29	0.0556	0.0309	0.0432	0.0375	0.0208	0.0291	0.4323	0.2400	0.3362
C30	0.0197	0.0322	0.0260	0.0133	0.0217	0.0175	0.1532	0.2505	0.2019
H31	0.0377	0.0314	0.0346	0.0254	0.0212	0.0233	0.2931	0.2444	0.2688
H32	0.0312	0.0290	0.0301	0.0210	0.0195	0.0203	0.2428	0.2252	0.2340
H33	0.0181	0.0008	0.0095	0.0122	0.0006	0.0064	0.1410	0.0066	0.0738
H34	0.0367	0.0331	0.0349	0.0247	0.0223	0.0235	0.2853	0.2577	0.2715
H35	0.0345	0.0288	0.0317	0.0233	0.0194	0.0213	0.2686	0.2237	0.2461

(*continued on next page*)

Table 8 (*continued*)

(b) The calculated Fukui functions, local softness and local eletrophilicity indices of 3OBC.

Atoms	f_k^+	f_k^-	f_k^0	S_k^+	S_k^-	S_k^0	ω_k^+	ω_k^-	ω_k^0
H36	0.0105	0.0190	0.0147	0.0071	0.0128	0.0099	0.0815	0.1477	0.1146
H37	0.0173	−0.0038	0.0068	0.0117	−0.0026	0.0046	0.1348	−0.0295	0.0526
H38	0.0476	0.0327	0.0401	0.0320	0.0220	0.0270	0.3697	0.2539	0.3118
H39	0.0479	0.0416	0.0447	0.0323	0.0280	0.0301	0.3721	0.3231	0.3476
H40	0.0422	0.0359	0.0391	0.0284	0.0242	0.0263	0.3281	0.2794	0.3037
H41	0.0094	0.0185	0.0140	0.0064	0.0125	0.0094	0.0734	0.1439	0.1087

Table 9

(a) Second order perturbation theory analysis of Fock matrix in NBO basis of 3OCE.

Donor(I)	Type of Band	Occupancy	Acceptor(J)	Type of Band	Occupancy	E2(Kj/mol)[a]	E(j)-E(i) (a.u)[b]	F(i, j) (a.u)[c]
C1-C2	π	1.69733	C3-C4	π*	0.30208	22.41	0.27	0.07
C1-C2	π	1.69733	C5-C6	π*	0.43606	19.34	0.24	0.063
C3-C4	π	1.67783	C1-C2	π*	0.28548	15.95	0.29	0.061
	π	1.67783	C5-C6	π*	0.02149	22.26	0.24	0.068
C5-C6	π	1.57918	C1-C2	π*	0.28548	18.96	0.29	0.069
	π	1.57918	C3-C4	π*	0.30208	16.12	0.28	0.062
	π	1.57918	C7-C8	π*	0.17173	24.74	0.21	0.07
C7-C8	π	1.76238	C5-C6	π*	0.43606	12.51	0.26	0.054
	π	1.76238	C9-O16	π*	0.27556	24.43	0.3	0.077
	π	1.76238	O17-C18	π*	0.21478	20.53	0.24	0.064
C7-H15	σ	1.97756	C8-C9	σ*	0.06404	12.61	0.43	0.067
C18-C19	σ	1.97936	C27-C28	σ*	0.01569	10.03	0.33	0.051
C19-C20	π	1.77557	O17-C18	π*	0.21478	25.14	0.23	0.068
	π	1.77557	C21-O22	π*	0.26996	17.58	0.27	0.062
	π	1.77557	C25-C26	π*	0.36714	11.92	0.31	0.056
C20-C21	σ	1.96426	C8-C9	σ*	0.06404	27.11	0.5	0.105
	σ	1.96426	C25-C26	σ*	0.02407	10.14	1.15	0.097
C20-C25	σ	1.96986	C8-C9	σ*	0.06404	15.19	0.56	0.083
C21-O22	σ	1.99468	C7-H15	σ*	0.01701	12.04	1.36	0.115
	σ	1.99468	C8-C9	σ*	0.06404	62.42	0.97	0.223
C21-N23	σ	1.98775	C4-C5	σ*	0.02149	79.72	1.17	0.274
	σ	1.98775	C7-H15	σ*	0.01701	50.5	1.14	0.214
	σ	1.98775	C8-C9	σ*	0.06404	288.47	0.75	0.419
	σ	1.98775	C18-C19	σ*	0.05302	51.79	1.15	0.22
	σ	1.98775	C27-C28	σ*	0.01569	395.09	0.5	0.398
	σ	1.98775	C29-H30	σ*	0.01374	30.45	2.54	0.249
N23-C24	σ	1.98561	C4-C5	σ*	0.02149	86.6	1.21	0.29
	σ	1.98561	C7-H15	σ*	0.01701	56.57	1.17	0.23
	σ	1.98561	C8-C9	σ*	0.06404	311.66	0.78	0.446
	σ	1.98561	C18-C19	σ*	0.05302	56.6	1.18	0.233
	σ	1.98561	C27-C28	σ*	0.01569	446.7	0.54	0.438
	σ	1.98561	C29-H30	σ*	0.01374	50.67	2.58	0.323
N23-H35	σ	1.98845	C1-H14	σ*	0.01336	23.48	0.56	0.102
	σ	1.98845	C4-C5	σ*	0.02149	33.34	0.5	0.115
	σ	1.98845	C7-H15	σ*	0.01701	24.48	0.46	0.095
	σ	1.98845	C8-C9	σ*	0.06404	606.52	0.07	0.186
	σ	1.98845	C18-C19	σ*	0.05302	32.21	0.47	0.111
	σ	1.98845	C29-H30	σ*	0.01374	43.41	1.87	0.254
C24-C25	σ	1.96108	C8-C9	σ*	0.06404	35.76	0.57	0.128
C24-C29	σ	1.97605	C4-C5	σ*	0.02149	22.27	1.05	0.137
	σ	1.97605	C7-C8	σ*	0.17173	10.01	0.67	0.076
	σ	1.97605	C7-H15	σ*	0.01701	14.49	1.01	0.108
	σ	1.97605	C8-C9	σ*	0.06404	87.53	0.62	0.21
	σ	1.97605	C18-C19	σ*	0.05302	12.71	1.02	0.103
	σ	1.97605	C27-C28	σ*	0.01569	30.02	0.38	0.095
C24-C29	π	1.66746	C25-C26	π*	0.36714	14.84	0.3	0.06
C25-C26	π	1.62799	C19-C20	π*	0.14243	17.32	0.29	0.067
	π	1.62799	C24-C29	π*	0.36651	24.24	0.27	0.073
C26-C27	σ	1.97623	C27-C28	σ*	0.01569	11.6	0.34	0.056
C26-H33	σ	1.97768	C27-C28	σ*	0.01569	19.03	0.16	0.049
C27-C28	π	1.66258	C24-C29	π*	0.36651	16.4	0.28	0.06
	π	1.66258	C25-C26	π*	0.36714	23.45	0.28	0.073
C28-H31	σ	1.98053	C8-C9	σ*	0.06404	21.02	0.43	0.085
	σ	1.98053	C27-C28	σ*	0.01569	91.52	0.18	0.116
	σ	1.97911	C8-C9	σ*	0.06404	38.34	0.42	0.115
	σ	1.97911	C27-C28	σ*	0.01569	53.02	0.18	0.087
C5-C6	π	0.43606	C1-C2	π*	0.28548	74.76	0.04	0.085
	π	0.43606	C3-C4	π*	0.01336	62.02	0.03	0.06
	π	0.43606	C21-O22	π*	0.26996	14.87	0.02	0.026
C7-C8	π	0.17173	C5-C6	π*	0.43606	162.88	0.04	0.123

(*continued on next page*)

Table 9 (*continued*)

Donor(I)	Type of Band	Occupancy	Acceptor(J)	Type of Band	Occupancy	E2(Kj/mol)[a]	E(j)-E(i) (a.u)[b]	F(i, j) (a.u)[c]
	π	0.17173	C9-O16	π*	0.27556	21.69	0.07	0.073
	π	0.17173	C21-O22	π*	0.26996	10.43	0.06	0.046
C9-O10	σ	0.1243	C5-O10	σ*	0.03292	11.92	0.05	0.077
O17-C18	π	0.21478	C5-C6	π*	0.43606	29.01	0.02	0.036
	π	0.21478	C19-C20	π*	0.14243	16.25	0.09	0.08
	π	0.21478	C21-O22	π*	0.26996	11.22	0.04	0.038
C21-O22	π	0.26996	C19-C20	π*	0.14243	23.89	0.05	0.067

(b) Second order perturbation theory analysis of Fock matrix in NBO basis of 3OBC.

Donor(I)	Type of Band	Occupancy	Acceptor(J)	Type of Band	Occupancy	E2(Kj/mol)[a]	E(j)-E(i) (a.u)[b]	F(i, j) (a.u)[c]
O12	LP(2)	1.766	C3-C4	π*	0.411	32.42	0.33	0.096
O12	LP(2)	1.766	C11-O13	π*	0.252	34.12	0.31	0.093
O13	LP(2)	1.844	C11-O12	σ*	0.118	41.51	0.49	0.128
O15	LP(2)	1.879	C10-C14	σ*	0.066	17.52	0.68	0.098
N24	LP(1)	1.773	C23-C28	π*	0.087	38.71	0.29	0.095
N24	LP(1)	1.773	C25-O26	π*	0.015	60.21	0.26	0.112
C1-C2	π	1.587	C3-C4	π*	0.411	16.68	0.25	0.059
	π	1.587	C5-C6	π*	0.292	17.64	0.27	0.065
	π	1.587	C17-C20	π*	0.147	16.46	0.27	0.063
	π	1.587	C18-C19	π*	0.144	17.18	0.28	0.065
C3-C4	π	1.646	C1-C2	π*	0.400	16.92	0.29	0.064
	π	1.646	C5-C6	π*	0.292	13.31	0.3	0.058
	π	1.646	C9-C10	π*	0.135	21.11	0.29	0.073
C5-C6	π	1.685	C1-C2	π*	0.400	14.2	0.29	0.06
	π	1.685	C3-C4	π*	0.411	21.32	0.28	0.071
C9-C10	π	1.789	C3-C4	π*	0.411	12.08	0.28	0.054
	π	1.789	C11-O13	π*	0.252	30.7	0.26	0.08
	π	1.789	C14-O15	π*	0.281	22.9	0.27	0.07
C9-H36	σ	1.979	C10-C11	σ*	0.066	5.52	0.99	0.067
C11-O13	π	1.981	C9-C10	π*	0.135	5.52	0.39	0.043
C14-O15	π	1.965	C16-C21	π*	0.150	6	0.4	0.045
C16-C21	σ	1.981	C21-C22	σ*	0.033	5.53	1.23	0.074
C16-C21	π	1.759	C14-O15	π*	0.281	24.3	0.25	0.07
	π	1.759	C22-C27	π*	0.028	12.05	0.3	0.056
	π	1.759	C25-O26	π*	0.015	18.8	0.26	0.063
C16-H41	σ	1.975	C21-C22	σ*	0.033	8.62	1	0.083
C17-C20	π	1.840	C1-C2	π*	0.400	18.61	0.28	0.067
	π	1.840	C18-C19	π*	0.144	17.4	0.29	0.063
C18-C19	π	1.841	C1-C2	π*	0.400	17.16	0.28	0.064
	π	1.841	C17-C20	π*	0.147	18.87	0.28	0.066
C22-C27	π	1.970	C16-C21	π*	0.150	17.63	0.28	0.066
	π	1.970	C23-C28	π*	0.087	24.05	0.26	0.071
	π	1.970	C29-C30	π*	0.029	16.83	0.27	0.061
C23-C28	π	1.987	C22-C27	π*	0.028	14.6	0.3	0.059
	π	1.987	C29-C30	π*	0.029	21.92	0.29	0.071
C27-C29	σ	1.768	C21-C22	σ*	0.033	5.02	1.17	0.069
C28-C30	σ	1.983	C23-N24	σ*	0.025	6.14	1.1	0.073
C29-C30	π	1.982	C22-C27	π*	0.028	23.15	0.28	0.072
	π	1.982	C23-C28	π*	0.087	16.93	0.27	0.061

[a] E2 means energy of hyper conjugative interactions.
[b] Energy difference between donor adn acceptor i. and j. NBO orbitals.
[c] F(i, j) is the Fock matrix element between i. and j. NBO orbitals.

Table 10
Interaction of 2IPM and 2IPL protein for both compounds 3OCE and 3OBC with docked energy.

Docked energy parameters	PDB-2IPM		PDB-2IPL	
	3OCE	3OBC	3OCE	3OBC
Binding_Energy (kcal/mol)	−8.85	−10.11	−8.22	−9.34
Ligand_Efficiency	−0.37	−0.36	−0.34	−0.33
Inhib_Constant	323.93 (nM)	38.61 (nM)	950.59 (nM)	142.22 (nM)
Intermol_Energy (kcal/mol)	−9.45	−10.71	−8.81	−9.94
Vdw_hb_desol_energy (kcal/mol)	−9.44	−10.63	−8.69	−9.92
Electrostatic _energy (kcal/mol)	−0.01	−0.08	−0.12	−0.02
Total_internal	−0.45	−0.52	−0.53	−0.6
Torsional_energy	0.6	0.6	0.6	0.6
Unbound_energy	−0.45	−0.52	−0.53	−0.6
Hydrogen Bond	GLN35, ALA258, ASN259, CYS70	GLN35, LYS285,	GLN35, MET38, LYS22	MET38, GLN26, LEU36, VAL232, SER18, LYS22, LYS285

References

[1] J.R. Lakowicz, Principle of Fluorescence Spectroscopy, Plenum Press, New York, 1983.
[2] K.K. Rohtagi–Mukherjee, Fundamentals of Photochemistry, Wiley Eastern Ltd., 1992.
[3] A.M. Musa, S.J. Cooper wood, M. Omar, F. Khan, Curr. Med. Chem. 15 (26) (2008) 2664–2679.
[4] Liang Lei, Yong-bo Xue, Zhong Liu, Si-si Peng, Yan He, Yang Zhang, Rong Fang, Jian-ping Wang, Zeng-wei Luo, Guang-min Yao, Jin-wen Zhang, Geng Zhang, Hong-ping Song, Yong-hui Zhang, Sci. Rep. 5 (2015), 13544.
[5] G. Collin, H. Höke, "Quinoline and Isoquinoline", Ullmann's Encyclopedia of Industrial Chemistry, Wiley-VCH, Weinheim, 2005, pp. a22–465.
[6] A. Kawski, B. Kuklinski, P. Bojarski, Chem. Phys. Lett. 448 (2007) 208–212.
[7] G.V. Muddapur, N.R. Patil, S.S. Patil, R.M. Melavanki, R.A. Kusanur, J. Fluoresc. 24 (6) (2014) 1651–1659.
[8] S.S. Patil, G.V. Muddapur, N.R. Patil, R.M. Melavanki, R.A. Kusanur, Spectrochim. Part A Mol. Biomol. Spectrosc. 138 (5) (2015) 85–91.
[9] E. Lippert, Z. Elektrochem. 61 (1957) 962–975.
[10] N.G. Bakshiev, Opt. Spectrosk. 16 (1964) 821–832.
[11] L. Bilot, A. Kawski, Z. Naturforsch. 18A (1963) 10–256. L. Bilot, A. Kawski, Z. Naturforsch., 17A (1962)- 621-627.
[12] A. Chamma, P. Viallet, C.R. Acad, Sci. Paris Ser. C 270 (1970) 1901–1904.
[13] A.R. Katritzky, D.C. Fara, H. Yang, K. Tamm, T. Tamm, M. Karelson, Chem. Rev. 104 (1) (2004) 175–198.
[14] C. Reichardt, Solvents and Solvent Effects in Organic Chemistry, 2nd, VCH, 1988.
[15] G.V. Muddapur, V.V. Koppal, N.R. Patil, R.M. Melavanki, AIP Conf. Proc. 1728 (2016), 020373.
[16] G.V. Muddapur, R.M. Melavanki, P.G. Patil, D. Nagaraja, N.R. Patil, J. Mol. Liq. 224 (2016) 201–210.
[17] V.V. Koppal, G.V. Muddapur, N.R. Patil, R.M. Melavanki, AIP Conf. Proc. 1728 (2016), 020411.
[18] V.R. Desai, A.H. Sidarai, S.M. Hunagund, M. Basanagouda, R.M. Melavanki, R. H. Fattepur, J.S. Kadadevarmath, J. Mol. Liq. 223 (2016) 141–149.
[19] V.V. Koppal, G.V. Muddapur, N.R. Patil, R.M. Melavanki, AIP Conf. Proc. 1728 (2016), 020411.
[20] Kalpana Sharma, Raveendra Melavanki, S.S. Patil, R.A. Kusanur, N.R. Patil, V. M. Shelar, J. Mol.Struct. 1181 (2019) 474–487.
[21] Elena Kirilova, Artur Yanichev, Aleksandrs Puckins, Mendel Fleisher, Sergey Belyakov, Luminescence (2018) 1–9.
[22] H.S. Geethanjali, D. Nagaraja, R.M. Melavanki, J. Fluoresc. 25 (3) (2015) 745–753.
[23] N.R. Patil, R.M. Melavanki, S.B. Kapatkar, N.H. Ayachit, J. Saravanan, J. Flurosec. 21 (2011) 1213–1222.
[24] R.M. Melavanki, H.D. Patil, S. Umapathy, J.S. Kadadevarmath, J. Fluoresc. 22 (2012) 137–144.
[25] J.S. Kadadevarmath, G.H. Malimath, N.R. Patil, H.S. Geethanjali, R.M. Melavanki, Can. J. Phys. 91 (2013) 1107–1113.
[26] P.G. Patil, V.V. Koppal, R.M. Melavanki, N.R. Patil, Mater. Today Proc. 5 (2018) 2781–2786.
[27] P. Bhavya, Raveendra Melavanki, M.N. Manjunatha, V.V. Koppal, N.R. Patiland, V. T. Muttannavar, AIP Conf. Proc. (1953), 080022-1–080022-080025.
[28] V.V. Koppal, P.G. Patil, R.M. Melavanki, N.R. Patil, Mater. Today Proc. 5 (2018) 2759–2764.
[29] P. Bhavya, Raveendra Melavanki, Kalpana Sharma, R. Kusanur, N.R. Patil, J. Thipperudrappa, Chem. Data Collect. 19 (2019), 100182.
[30] Nejla Khatir–Hamdi, Malika Makhloufi-Chebli, Hocine Grib, M. éziane Brahimi, Artur M.S. Silva, J. Mol. Struct. 1175 (2019) 811–820.
[31] Yadigar Gulseven Sıdır, Isa Sıdır, Spectrochim. Acta Part A 102 (2013) 286–296.
[32] M.S. Zakerhamidi, S. Ahmadi-Kandjani, M. Moghadam, E. Ortyl, S. Kucharski, J. Mol. Struct. 996 (2011) 95–100.
[33] Ghanadzadeh Gilani, S.E. Hosseini, M. Moghadam, E. Alizadeh, Spectrochim. Acta Part A 89 (2012) 231–237.
[34] Gaddam Ramesh, Byru Venkatram Reddy, J. Mol. Struct. 1160 (15) (2018) 271–292.
[35] Mostafa Khajehzadeh, Nasrin Sad, J. Mol.Liq. 249 (2018) 281–293.
[36] Nuha A. Wazzan, Ohoud S. Al-Qurashi, H.M. Faidallah, J. Mol. Liq. 223 (2016) 29–47.
[37] R. Srivastava, F.M. Al-Omary, Ali A. El-Emam, S.K. Pathak, M. Karabacak, Vijay Narayan, Satish Ch, Onkar Prasad, Leena Sinha, J. Mol. Struct. 1137 (5) (2017) 725–741.
[38] Khairia M. Al-Ahmary, Ramadan Ahmed Mekheimer, Maha S. Al-Enezi, Nagwa M. M. Hamada, Moustafa M. Habeeb, J. Mol. Liq. 249 (2018) 501–510.
[39] Dhanraj R. Mohbiya, Nagaiyan Sekar, Chem. Select. 3 (2018) 1635–1644.
[40] Hasan Tanak, Ays En Agar, Metinyavuz, Int. J. Quant. Chem. 111 (2011) 2123–2136.
[41] S. Premkumar, A. Jawahar, T. Mathavan, M. Kumara Dhas, A. Milton Franklin Benial, Spectrochim. Acta Part A. 138 (2015) 252–263.
[42] S. Premkumar, A. Jawahar, T. Mathavan, M. Kumara Dhas, V.G. Sathe, A. Milton Franklin Benial, Spectrochim. Acta Part A 129 (2014) 74–83.
[43] S. Premkumar, T.N. RekhaBeulah, J.M. Rajkumar, R. Mohamed Asath, A. Jawahar, T. Mathavan, A. Milton Franklin Benial, Braz. J. Phys. 45 (6) (2015) 621–632.
[44] S. Premkumar, T.N. Rekha, R. Mohamed Asath, T. Mathavan, A. Milton Franklin Benial, Euro. J. Pharma. Sc. 82 (2016) 115–125.
[45] S. Premkumar, T.N. Rekha, R. Mohamed Asath, A. Jawahar, T. Mathavan, A. Milton Franklin Benial, J. Mol. Struct. 1107 (2016) 254–265.
[46] V.T. Muttannavar, R. Melavanki, P. Bhavya, R. Kusanur, N.R. Patil, L.R. Naik, Int. J. Life Sci. Phar. Res. 8 (3) (2018) 24–30.
[47] M.J. Frisch, G.W. Trucks, H.B. Schlegel, G.E. Scuseria, M.A. Robb, J.R. Cheeseman, G. Scalmani, V. Barone, B. Mennucci, G.A. Petersson, et al., Gaussian 09 RA. 1, Gaussian. Inc., Wallingford CT, 2009.
[48] A. Frisch, A.B. Nielsen, A.J. Holder, Gaussview User Manual, Gaussian Inc., Pittsburgh, PA, 2000, p. 556.
[49] R. Dengton, T. Keith, J. Millam, K. Eppinnett, W.L. Hovell, R. Gilliland, GaussView, Version 309, Semichem, Inc, Shawnee Mission, KS, 2003.
[50] E.D. Glendening, A.E. Reed, J.E. Carpenter, F. Weinhold, NBO Version 3.1, TCI. University of Wisconsin, Madison, 1998, p. 65.
[51] C. Wohlfarth, Static Dielectric Constants of Pure Liquids and Binary Liquid Mixtures: Supplement to IV/6, Springer Science & Business Media, 2008.
[52] P. Suppan, C. Tsiamis, Spectrochim. ActaPartA 36 (1980) 971–974. Suppan, J. Chem. Soc. A 3125 (1968).
[53] C. Reichardt, Chem. Rev. 94 (1994) 2319–2358.
[54] M. Ravi, T. Soujnya, A. Samanta, T.P. Radhakrishnan, J. Chem. Soc. Faraday Trans. 91 (1995) 2739–2742.
[55] S. Premkumar, T.N. Rekha, R. Mohamed Asath, T. Mathavan, A. Milton Franklin Benial, Eur. J. Pharm. Sci. 82 (2016) 115–125.
[56] S. Premkumar, T.N. Rekha, R. Mohamed Asath, A. Jawahar, T. Mathavan, A. Milton Franklin Benial, J. Mol. Struct. 1107 (2016) 254–265.
[57] Zeynep Demircioğlu, Çiğdem Albayrak Kaştaş, Orhan Büyükgüngör, Spectrochim. Acta A. Mol. Biomol. Spectrosc. 15 (3) (2015) 539–548.
[58] Edina H. Avdović, Dejan Milenković, Jasmina M.Dimitrić Marković, Jelena Đorović, Nenad Vuković, Milena D. Vukić, Verica V. Jevtić, Srećko R. Trifunović, Ivan Potočňák, Zoran Marković, Spectrochim. Acta A Mol. Biomol. Spectrosc. 195 (4) (2018) 31–40.
[59] R.G. Parr, W. Yang, Density functional approach to the frontier-electron theory of chemical reactivity, J. Am. Chem. Soc. 106 (1984) 4049–4050.
[60] K. Fukui, Theory of Orientation and Stereoselection, Springer-Verlag, Berlin, 1975.
[61] L.I.U. Shu-BIN, Conceptual density functional theory and some recent developments, Acta Phys. ChimSin. 25 (2009) 590–600.
[62] http://www.molinspiration.com/cgi-bin/properties.
[63] R.A. Kusanur, M.V. Kulkarni, Asian J. Chem. 26 (4) (2014) 1077.
[64] R. Kalirajan, M. Pandiselvi, S. Sankar, B. Gowramma, S F J. Pharma. Anal. Chem. (2018). Science Forecast Publications LLC., | https://scienceforecastoa.com/ 2018 Volume 1 Edition 1 Article 1004.
[65] Dayanand Patagar, Raviraj Kusanur, Nikum D. Sitwala, Manjunath D. Ghate, Shanmugasundar Saravanakumar, Sharanappa Nembenna, Piyush A. Gediya, J. Heterocycl. Chem. 56 (10) (2019) 2761–2771.
[66] Amal Al Sabahi, Saleh N. Al Busafi, Fakhr Eldin O. Suliman, Salma M. Al Kindy, J. Mol. Liq. 307 (1) (2020), 112967.